NISKINE Microstructure Data Report: 8 AUG 2020

E. Kunze and R.-C. Lien

During the NISKINE process cruise, arrays of up to 15 chi-augmented EM-APEX profiling floats were deployed on 3 occasions during 29 MAY-17 JUN (Fig. 5). Six floats were left at sea for extended sampling over the longer term (Fig. 6). As of 3 AUG 2020, 3 were still reporting back but only 7806 is still providing microstructure data. Of the other 5, one stopped reporting microstructure reliably in late SEP 2019, 2 in NOV 2019, 1 at the end of JAN 2020 and 1 at the end of MAR 2020 (Fig. 6).

Here is summary of EM float microstructure analysis after some back and forth with Ren-Chieh Lien. Table 1 summarizes data quality by float, chi sensor and drop number (hpid). These selections are based on examination of sensor pdfs (e.g., Fig. 7), time-average depth profiles (e.g., Fig. 8) and sensor profile time-series (e.g., Figs. 5 and 6). Bad data include chi2 for 4969, chi1 for 4970, chi1 for 4971, epsilon1 for 7488, chi1 for 7802, chi1 for 7803, chi2 for 7805, chi2 for 7806, chi1 for 7808, both sensors for 4967 hpid ≤ 36, chi1 for 4969 hpid ≥ 771, chi2 for 4971 hpid ≥ 240, chi1 for 7807 hpid ≥ 314, chi 2 for 7807 hpid ≥ 160 and chi2 for 7808 hpid ≥ 196. Also the first 5 estimates of each rising profile have been excluded from averages below.

Fig. 1 shows the total PDFs of measured thermal variance dissipation rate χ_T, inferred TKE dissipation rate ε and thermal diffusivity K_T from all the floats' time-series. Not included are data as indicated in Table 1, and where $N^2 < 4f^2$, $T_z < 2 \times 10^{-3}$ °C/m (to remove unreliable χ_T, ε and K_T). Outliers ($\chi_T > 10^{-5}$ °C^2 s^{-1}, $\varepsilon > 10^{-6}$ W kg^{-1}, $K_T > 10^{-2}$ m^2 s^{-1}) are also excluded in subsequent averages. Mean (mode) TKE dissipation rates ε are 2.8×10^{-9} (10^{-10}) W kg^{-1}. Mean (mode) thermal diffusivities K_T are 0.56×10^{-4} (~0.1×10^{-4}) m^2 s^{-1}. This indicates that the outliers are about 3 standard deviations in log space above the mode. Statistics for the JUN 2019 process cruise are similar (see Appendix B). Mean diffusivities from individual floats ranged over (0.3-0.8) $\times 10^{-4}$ m^2 s^{-1} and dissipation rates (1.3-4.0) $\times 10^{-9}$ W kg^{-1} (Fig. 7; Appendix B). Average dissipation rates and diffusivities decrease with depth with no dip in ε associated with the mode-water N minimum at 150-400 m depth(Fig. 2).

Time-series of depth- and float-averaged thermal variance dissipation rate χ_T, TKE dissipation rate ε and thermal diffusivity K_T for the June 2019 process cruise and longterm record (Fig. 3) summarize temporal behavior. Average diffusivities $K_T \sim (0.5\text{-}0.8) \times 10^{-4}$ m^2 s^{-1} and TKE dissipaton rates $\varepsilon \sim (2\text{-}3) \times 10^{-9}$ W kg^{-1} during the process cruise. The longterm record exhibits order-of-magnitude variability with peaks in SEP, JAN and APR, and valleys in JUL-AUG, OCT and MAR; peaks in JAN may be due to high χ_T in the mixed layer from which ε and K_T may not be reliable. K_T varies from 0.2 to 5×10^{-4} m^2 s^{-1}. Dissipation rates ε vary from 1 to 6×10^{-9} W kg^{-1}. A map of depth-averaged thermal diffusivity K_T largely reflects space-time aliasing (Fig. 4).

Fine- and microstructure profile time-series of N, T_z, χ_T, ε and K_T are shown for each float in Appendix A [Figs. 5 (process cruise) and 6 (longterm)]. Floats 4971 and 7807 exhibited abrupt changes in microstructure, coincident with changes in finescale water-mass structure, in the latter half of NOV 2019 (not shown). Since there is only 1 reliable chi sensor in each case, these changes are impossible to verify.

Appendix B shows PDFs, time-average profiles and depth-average time-series by sensor.

Table 1: Data quality by float, sensor and drop number (hpid). Float number prefixed by * were left in the water after the process cruise. Good hpid profiles are denoted.

float	**chi1**	**chi2**
4966	OK	OK
4967	hpid > 36	hpid>36
4968	OK	OK
*4969	hpid < 771	BAD
4970	BAD	OK
*4971	BAD	hpid<240
7488	epsilon BAD	OK
7801	OK	OK
*7802	BAD	OK
7803	BAD	OK
7804	OK	OK
7805	OK	BAD
*7806	OK	BAD
*7807	hpid < 314	hpid<160?
*7808	BAD	hpid<196

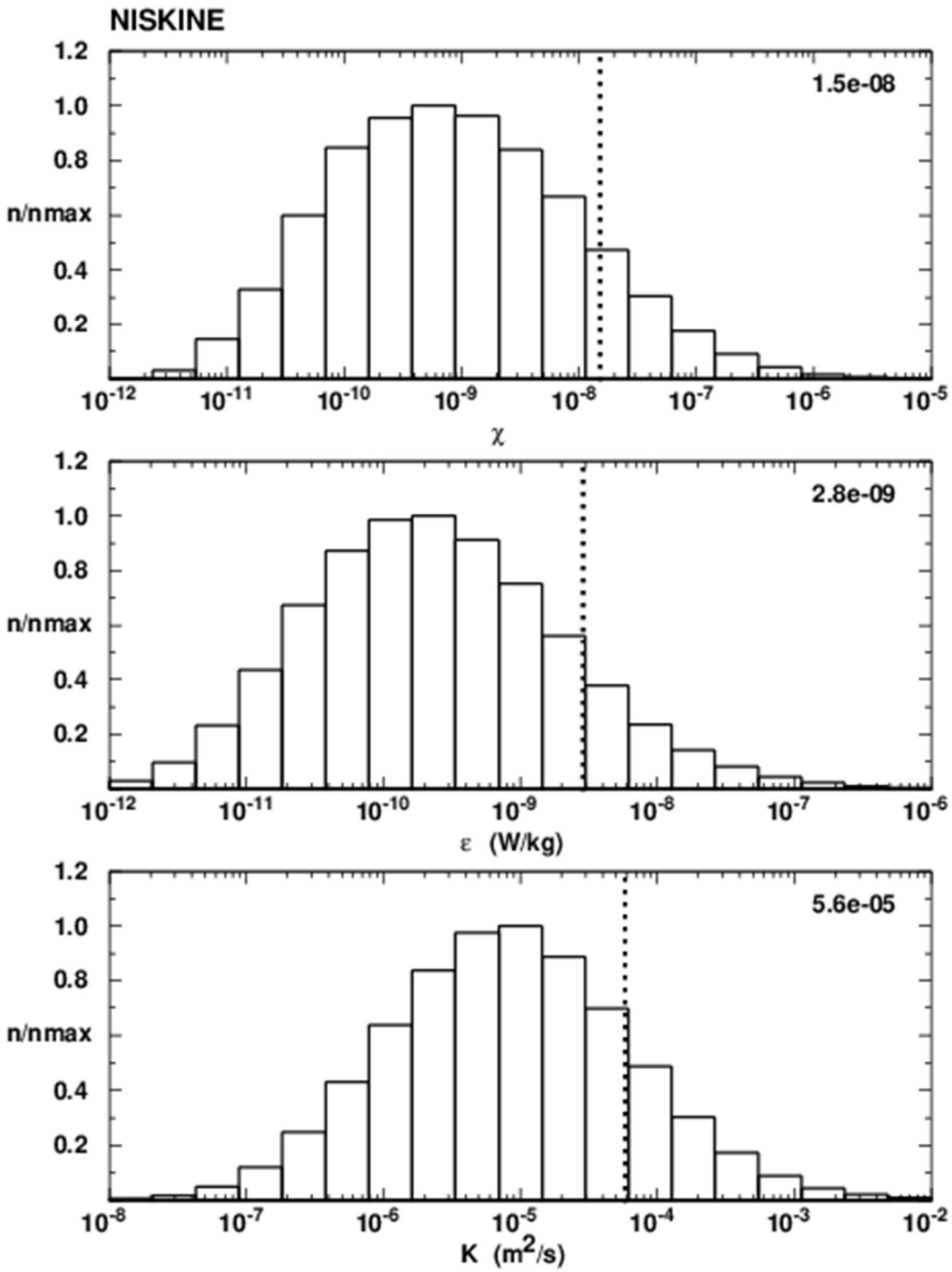

Figure 1: PDFs of thermal variance dissipation rate χ_T (°C^2/s), TKE dissipation rate ε and thermal diffusivity K_T from all the NISKINE EM float data. All the distributions appear log-normal. Means for these PDFs are indicated by the dotted vertical lines and numbers.

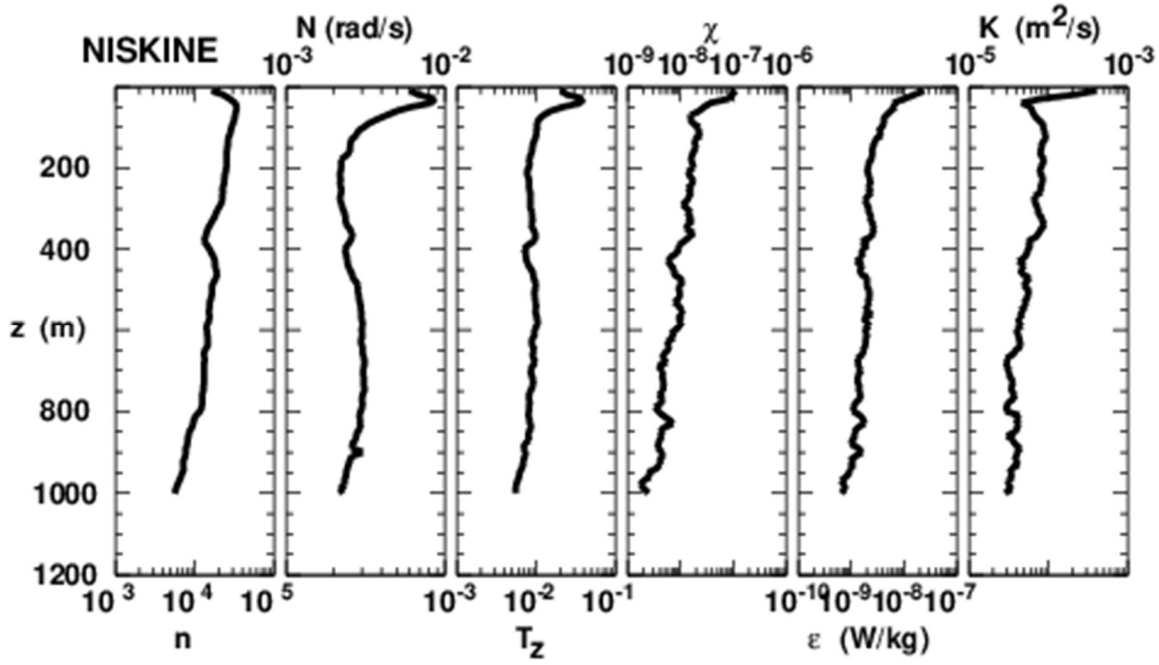

Fig. 2: Profiles of number of data points going into the float- and time- averages n, as well as average buoyancy frequency N (rad/s), temperature-gradient T_z (°C/m), thermal-variance dissipation rate χ_T (°C^2/s), TKE dissipation rate ε (W kg^{-1}) and thermal diffusivity K_T (m^2 s^{-1}) from the NISKINE EM float measurements.

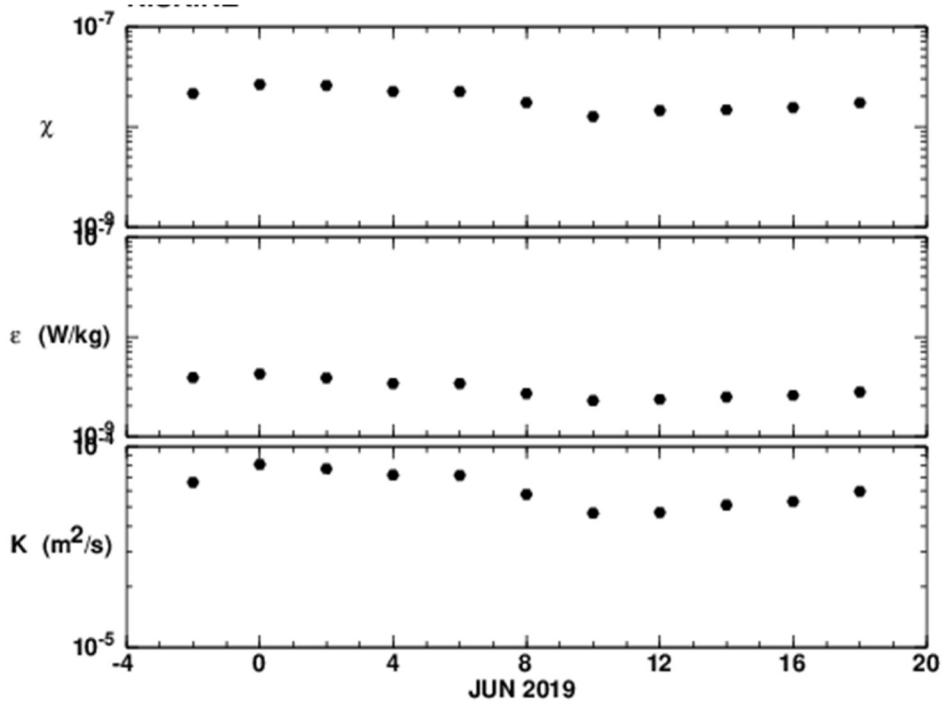

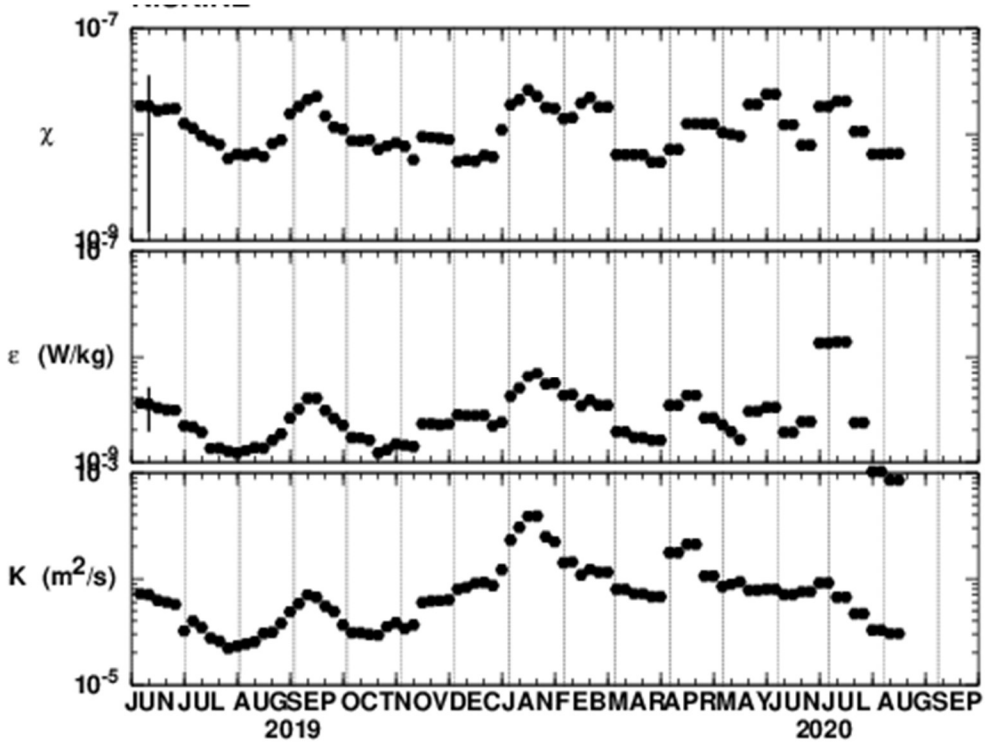

Fig. 3: Time-series of depth- and float-averaged thermal variance dissipation rate χ_T (°C^2/s) TKE dissipation rate ε and thermal diffusivity K_T for the June 2019 process cruise, which sees weak decreases over the sampling interval, and longterm record which exhibits order of magnitude variability with peaks in SEP, JAN and APR, and valleys in JUL-AUG, OCT and MAR. Data were not included in the average if the sensor failed, as well as $N^2 < 4f^2$ or $T_z < 0.002$ C/m.

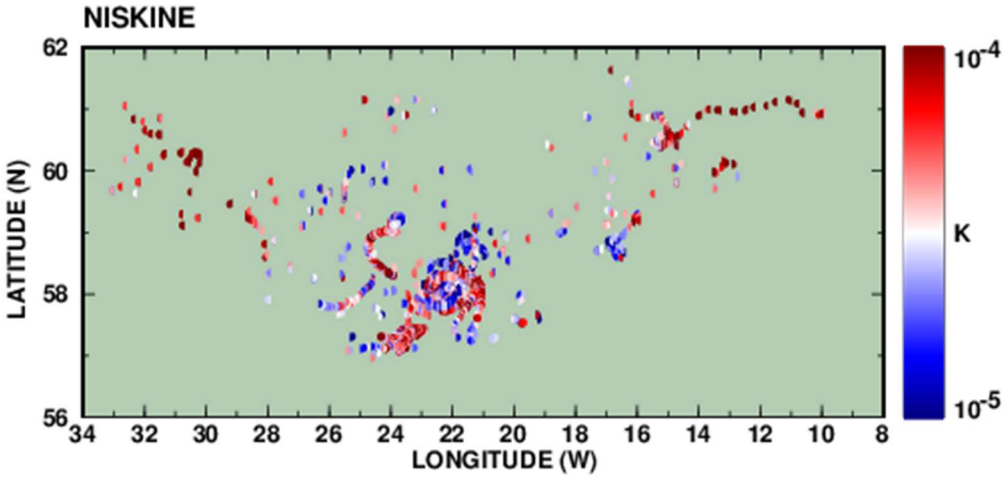

Fig. 4: Map of depth-average thermal diffusivity K_T (m^2 s^{-1}). Compare with Fig. 3 for space-time aliasing.

Appendix A: Profile Time-Series for Each Float: .

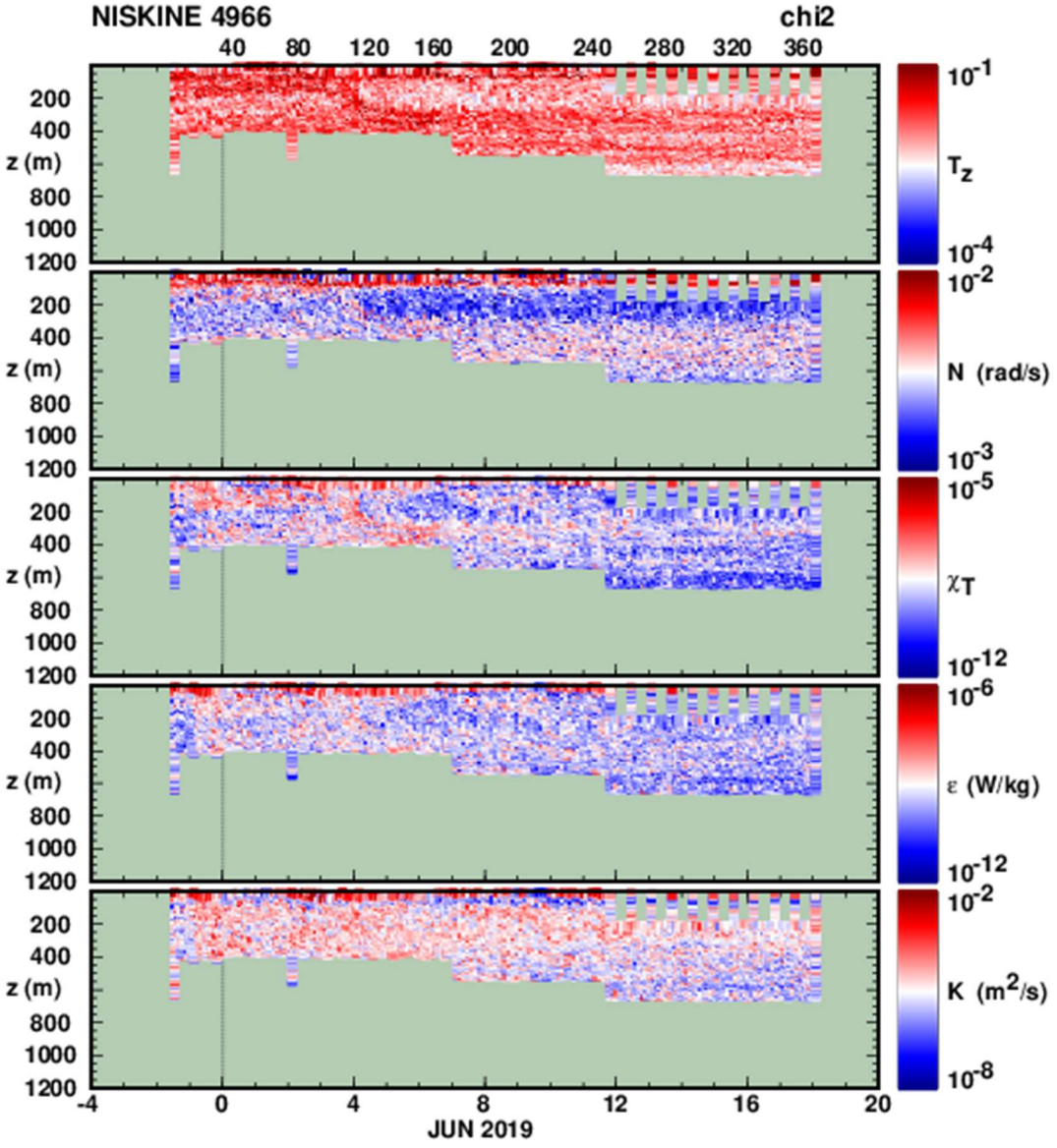

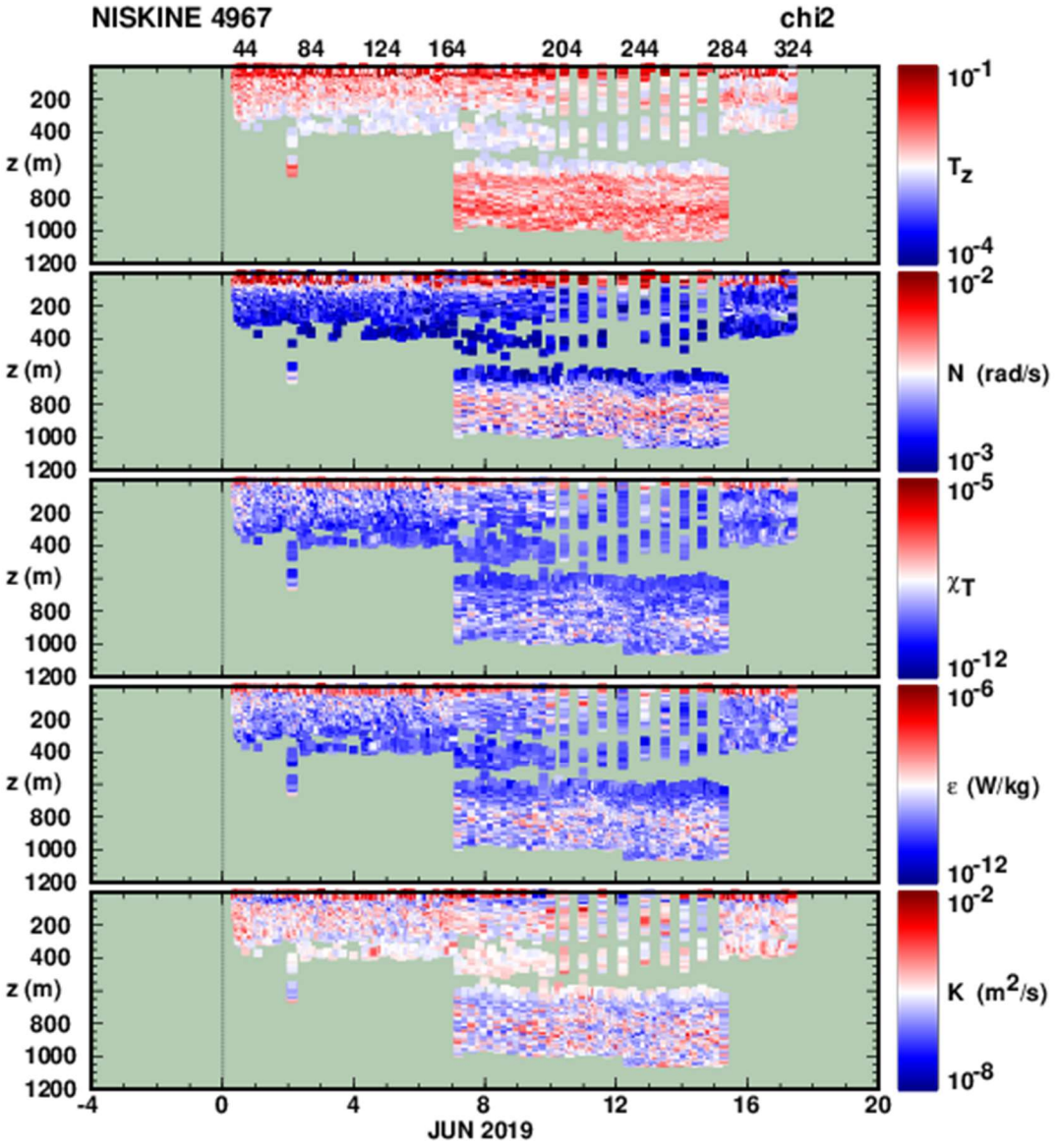
NISKINE 4967
chi2
44
84
124
164
204
244
284
324
z (m)
200
400
800
1000
1200
10^{-1}
T_z
10^{-4}
10^{-2}
N (rad/s)
10^{-3}
10^{-5}
χ_T
10^{-12}
10^{-6}
ε (W/kg)
10^{-12}
10^{-2}
K (m^2/s)
10^{-8}
-4
0
4
8
12
16
20
JUN 2019

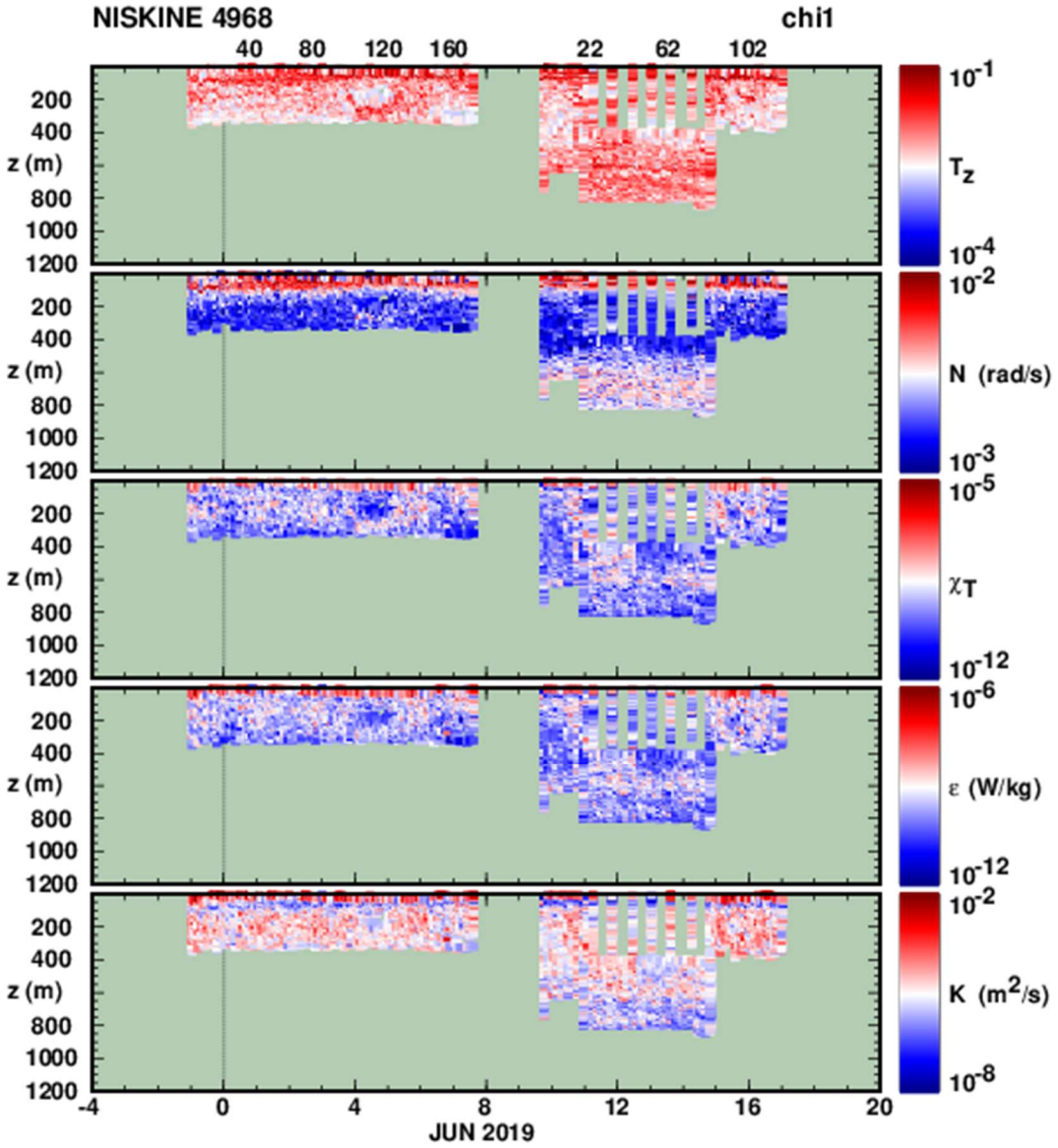
NISKINE 4968
chi1
40
80
120
160
22
62
102
z (m)
200
400
800
1000
1200
10^{-1}
T_z
10^{-4}
10^{-2}
N (rad/s)
10^{-3}
10^{-5}
χ_T
10^{-12}
10^{-6}
ε (W/kg)
10^{-12}
10^{-2}
K (m^2/s)
10^{-8}
-4
0
4
8
12
16
20
JUN 2019

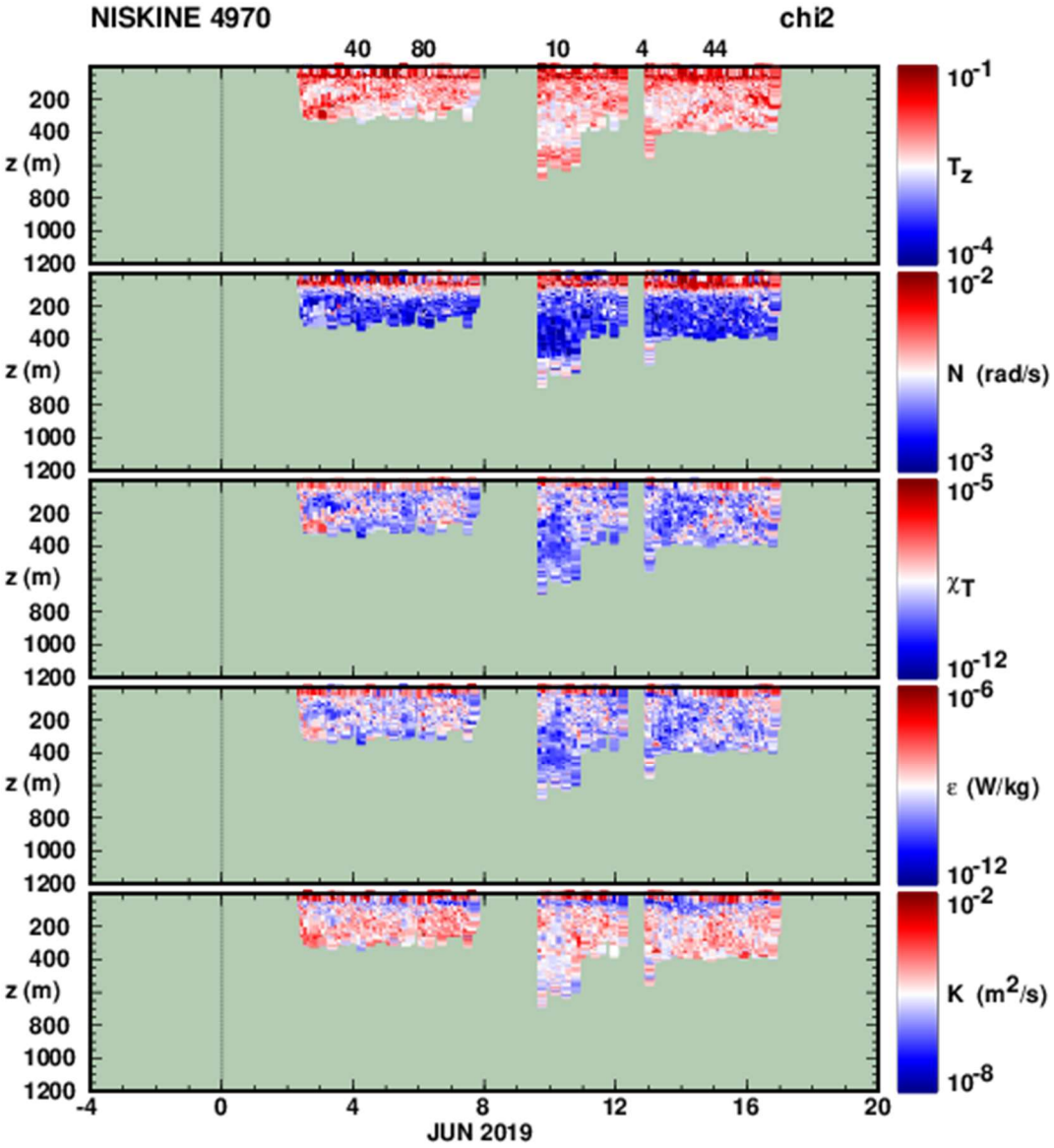
NISKINE 4970
chi2
40
80
10
4
44
z (m)
200
400
800
1000
1200
10^{-1}
T_z
10^{-4}
10^{-2}
N (rad/s)
10^{-3}
10^{-5}
χ_T
10^{-12}
10^{-6}
ε (W/kg)
10^{-12}
10^{-2}
K (m^2/s)
10^{-8}
-4
0
4
8
12
16
20
JUN 2019

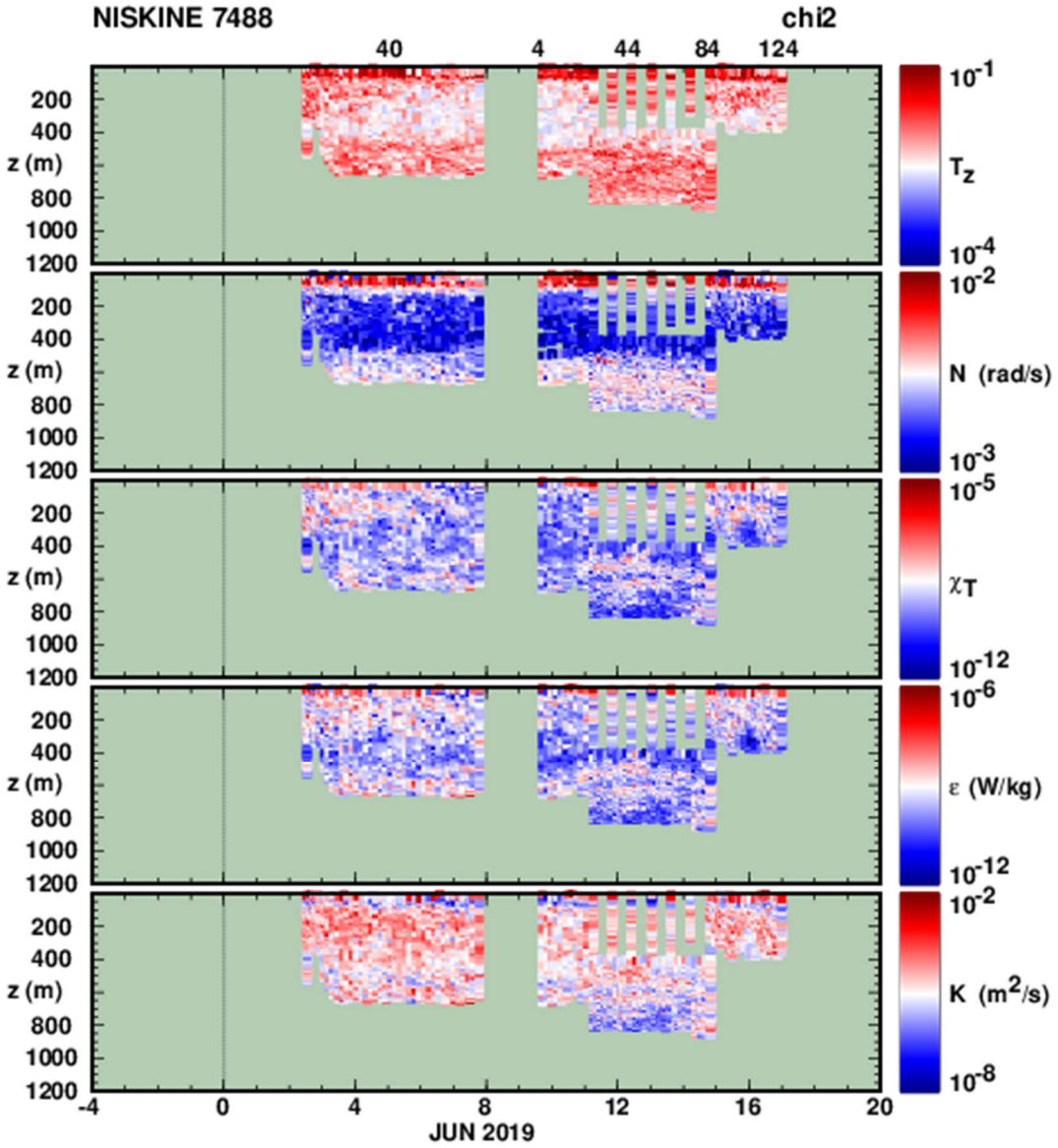
NISKINE 7488
chi2
40
4
44
84
124
z (m)
200
400
800
1000
1200
10^{-1}
T_z
10^{-4}
10^{-2}
N (rad/s)
10^{-3}
10^{-5}
χ_T
10^{-12}
10^{-6}
ε (W/kg)
10^{-12}
10^{-2}
K (m^2/s)
10^{-8}
-4
0
4
8
12
16
20
JUN 2019

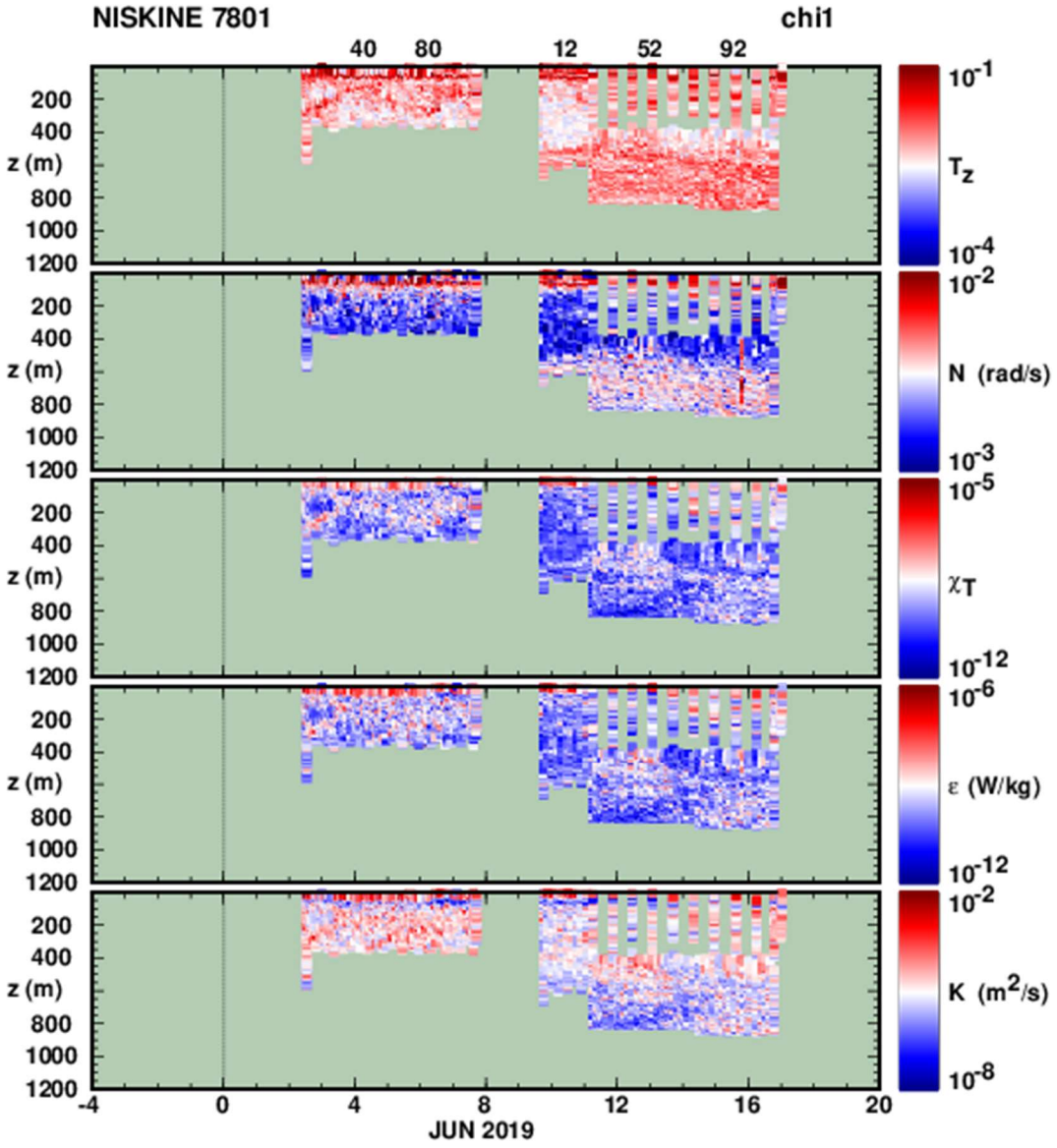
NISKINE 7801
chi1
40
80
12
52
92
z (m)
200
400
800
1000
1200
10^{-1}
T_z
10^{-4}
10^{-2}
N (rad/s)
10^{-3}
10^{-5}
χ_T
10^{-12}
10^{-6}
ε (W/kg)
10^{-12}
10^{-2}
K (m^2/s)
10^{-8}
-4
0
4
8
12
16
20
JUN 2019

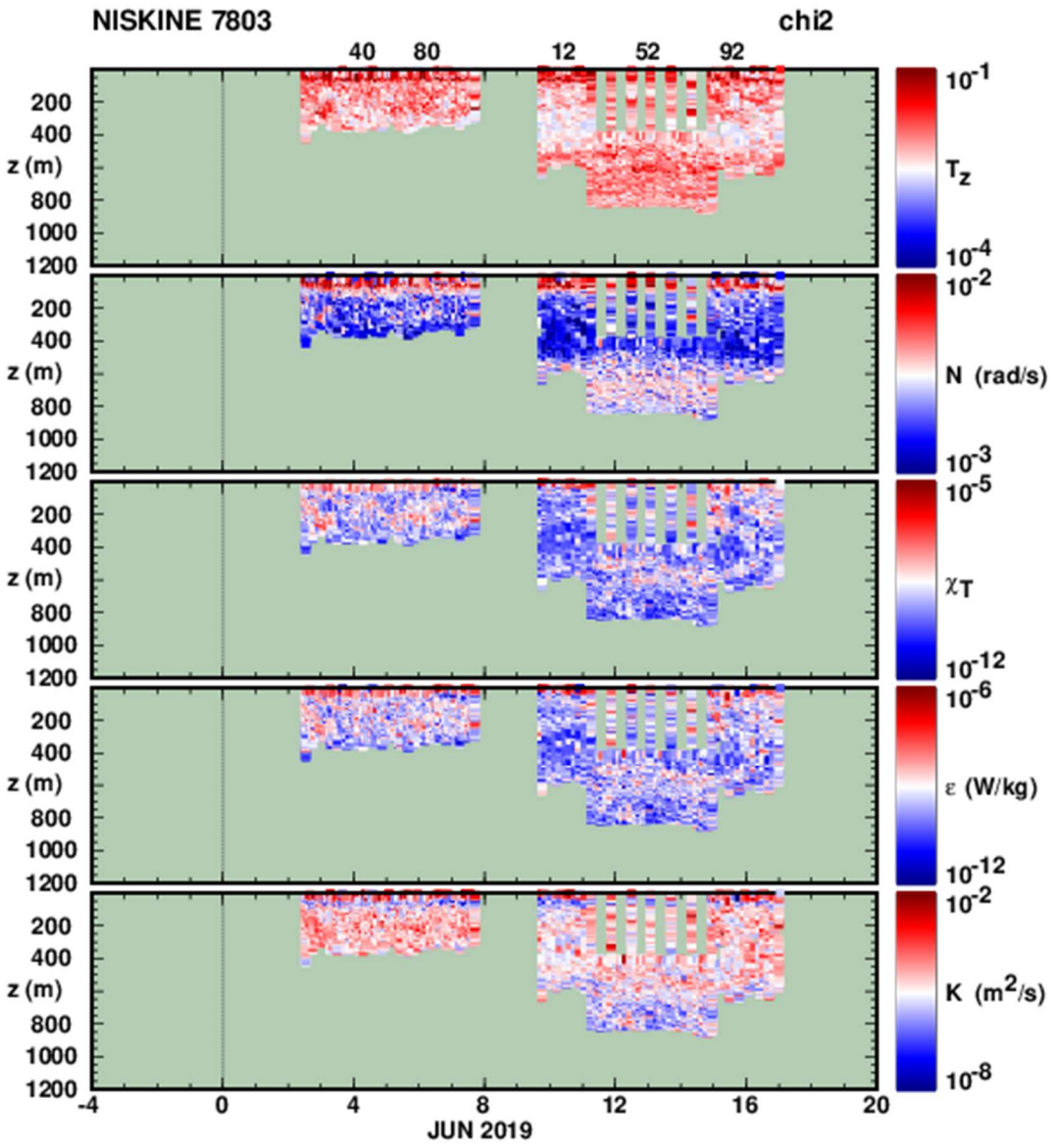
NISKINE 7803
chi2
40
80
12
52
92
z (m)
200
400
800
1000
1200
10^{-1}
T_z
10^{-4}
10^{-2}
N (rad/s)
10^{-3}
10^{-5}
χ_T
10^{-12}
10^{-6}
ε (W/kg)
10^{-12}
10^{-2}
K (m^2/s)
10^{-8}
-4
0
4
8
12
16
20
JUN 2019

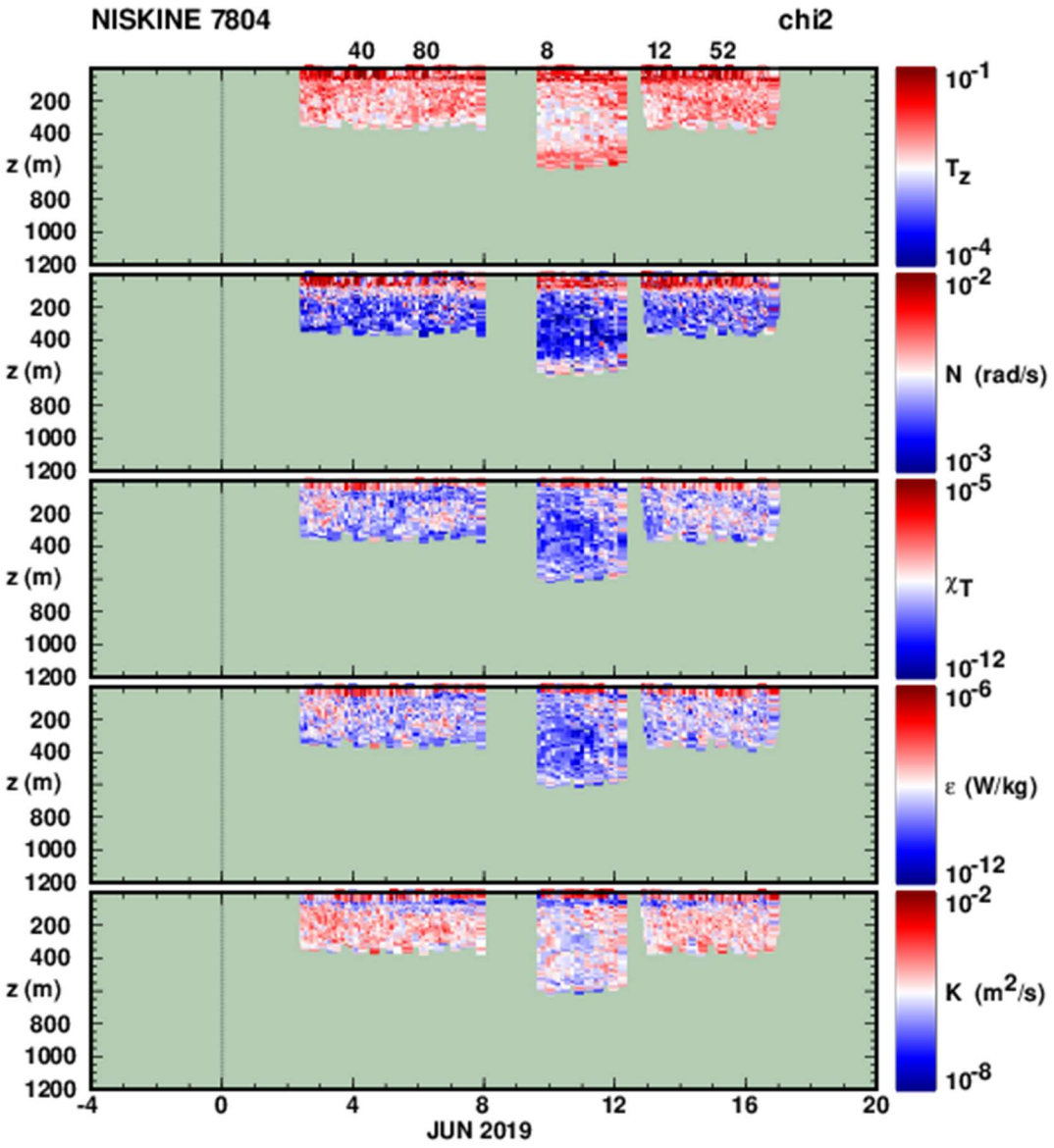
NISKINE 7804
chi2
40
80
8
12
52
z (m)
200
400
800
1000
1200
10^{-1}
T_z
10^{-4}
10^{-2}
N (rad/s)
10^{-3}
10^{-5}
χ_T
10^{-12}
10^{-6}
ε (W/kg)
10^{-12}
10^{-2}
K (m^2/s)
10^{-8}
-4
0
4
8
12
16
20
JUN 2019

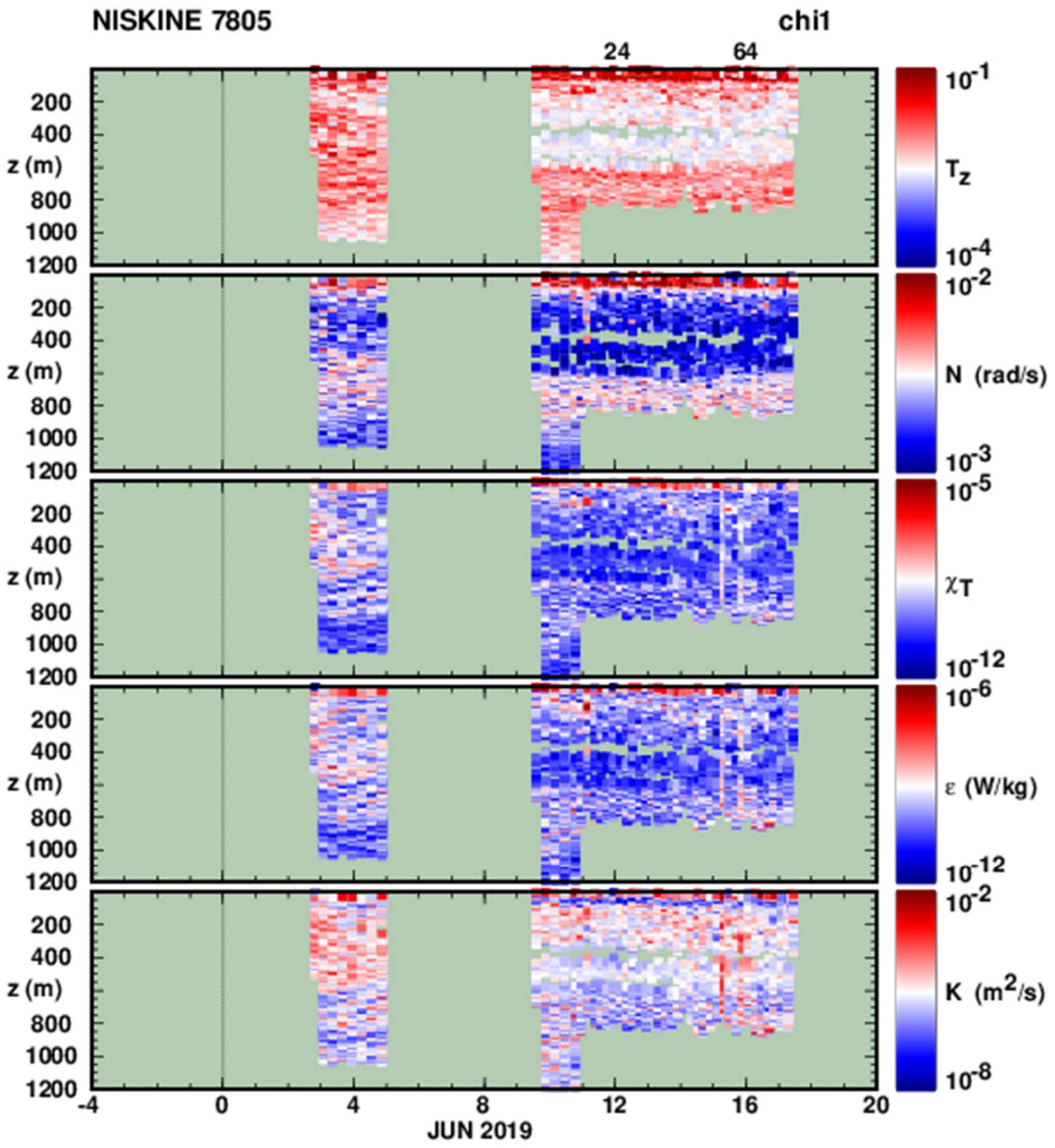

Fig. 5: Profile time-series of finescale vertical temperature-gradient T_z, buoyancy frequency N, thermal variance dissipaton rate χ_T, TKE dissipation rate ε and thermal diffusivity K_T from the 9 EM floats only deployed during the JUN 2019 process cruise. The chi sensor displayed (above right upper axis) was the one that appeared to provide the best data.

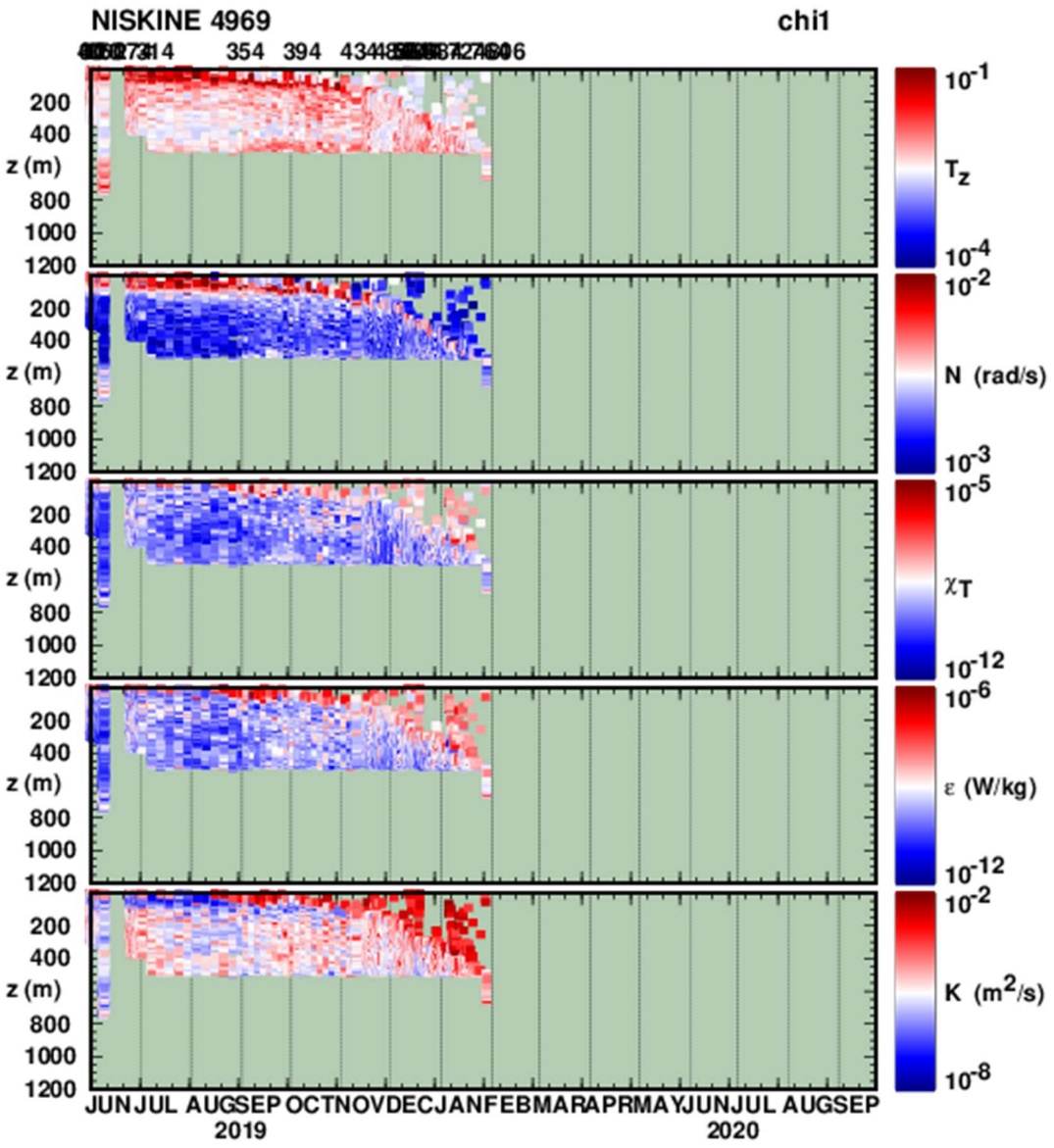
NISKINE 4969
chi1
354
394
z (m)
200
400
800
1000
1200
JUN JUL AUG SEP OCT NOV DEC JAN FEB MAR APR MAY JUN JUL AUG SEP
2019
2020
10^{-1}
T_z
10^{-4}
10^{-2}
N (rad/s)
10^{-3}
10^{-5}
χ_T
10^{-12}
10^{-6}
ε (W/kg)
10^{-12}
10^{-2}
K (m^2/s)
10^{-8}

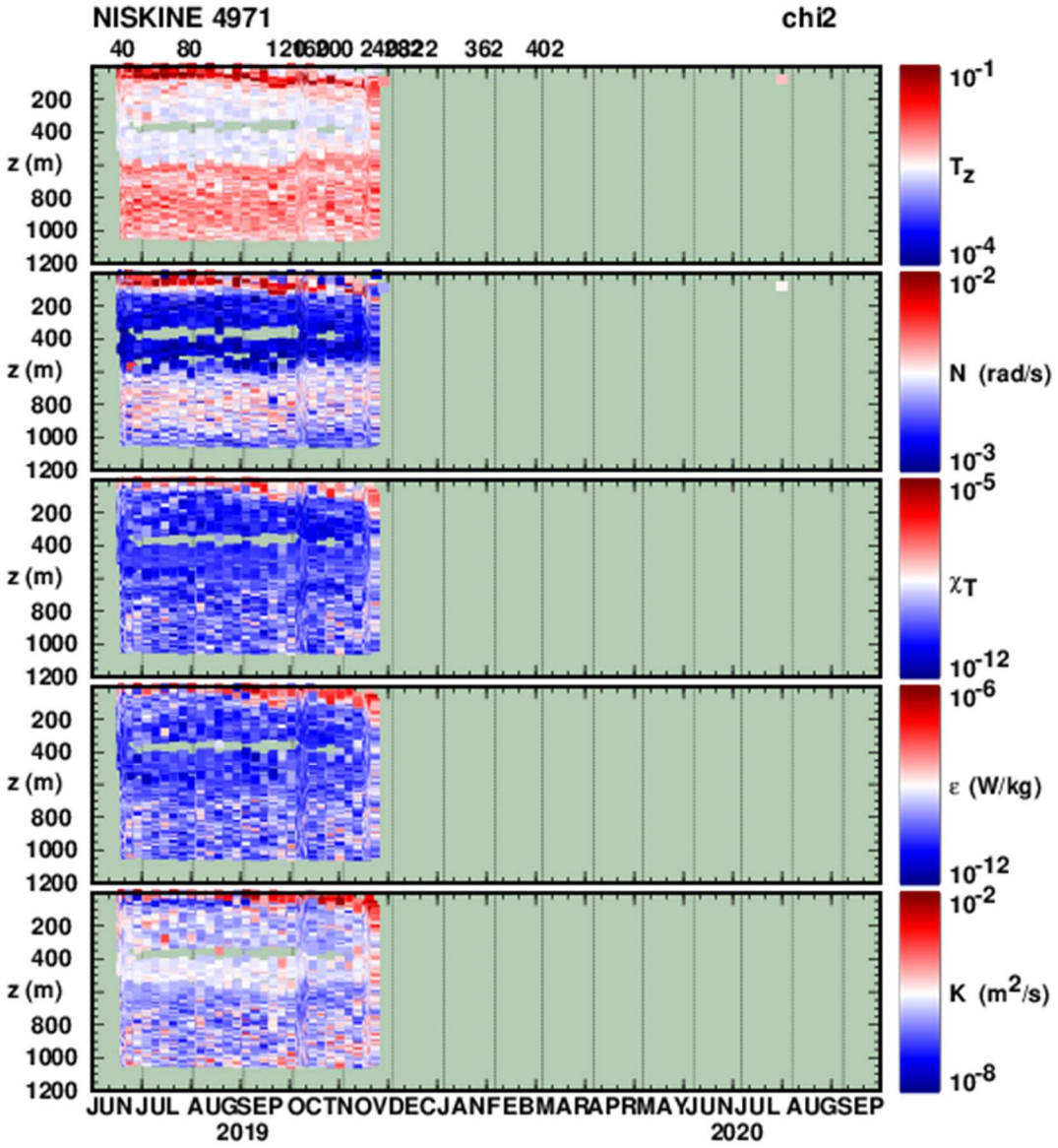
NISKINE 4971
chi2
40
80
362
402
z (m)
200
400
800
1000
1200
10^{-1}
T_z
10^{-4}
10^{-2}
N (rad/s)
10^{-3}
10^{-5}
χ_T
10^{-12}
10^{-6}
ε (W/kg)
10^{-12}
10^{-2}
K (m^2/s)
10^{-8}
JUN JUL AUG SEP OCT NOV DEC JAN FEB MAR APR MAY JUN JUL AUG SEP
2019
2020

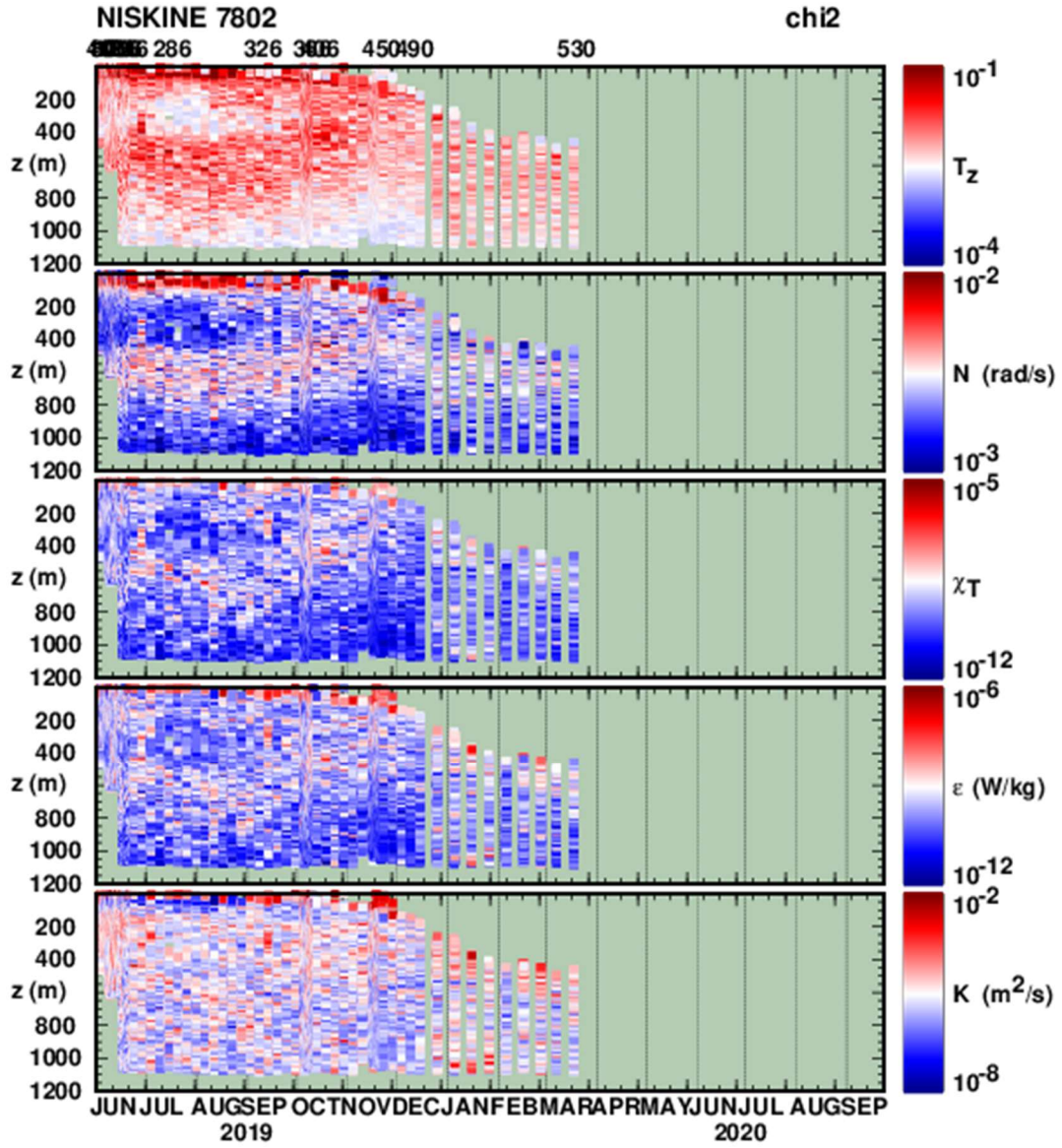
NISKINE 7802
chi2
286
326
450
490
530
z (m)
200
400
800
1000
1200
10^{-1}
T_z
10^{-4}
10^{-2}
N (rad/s)
10^{-3}
10^{-5}
χ_T
10^{-12}
10^{-6}
ε (W/kg)
10^{-12}
10^{-2}
K (m^2/s)
10^{-8}
JUN JUL AUG SEP OCT NOV DEC JAN FEB MAR APR MAY JUN JUL AUG SEP
2019
2020

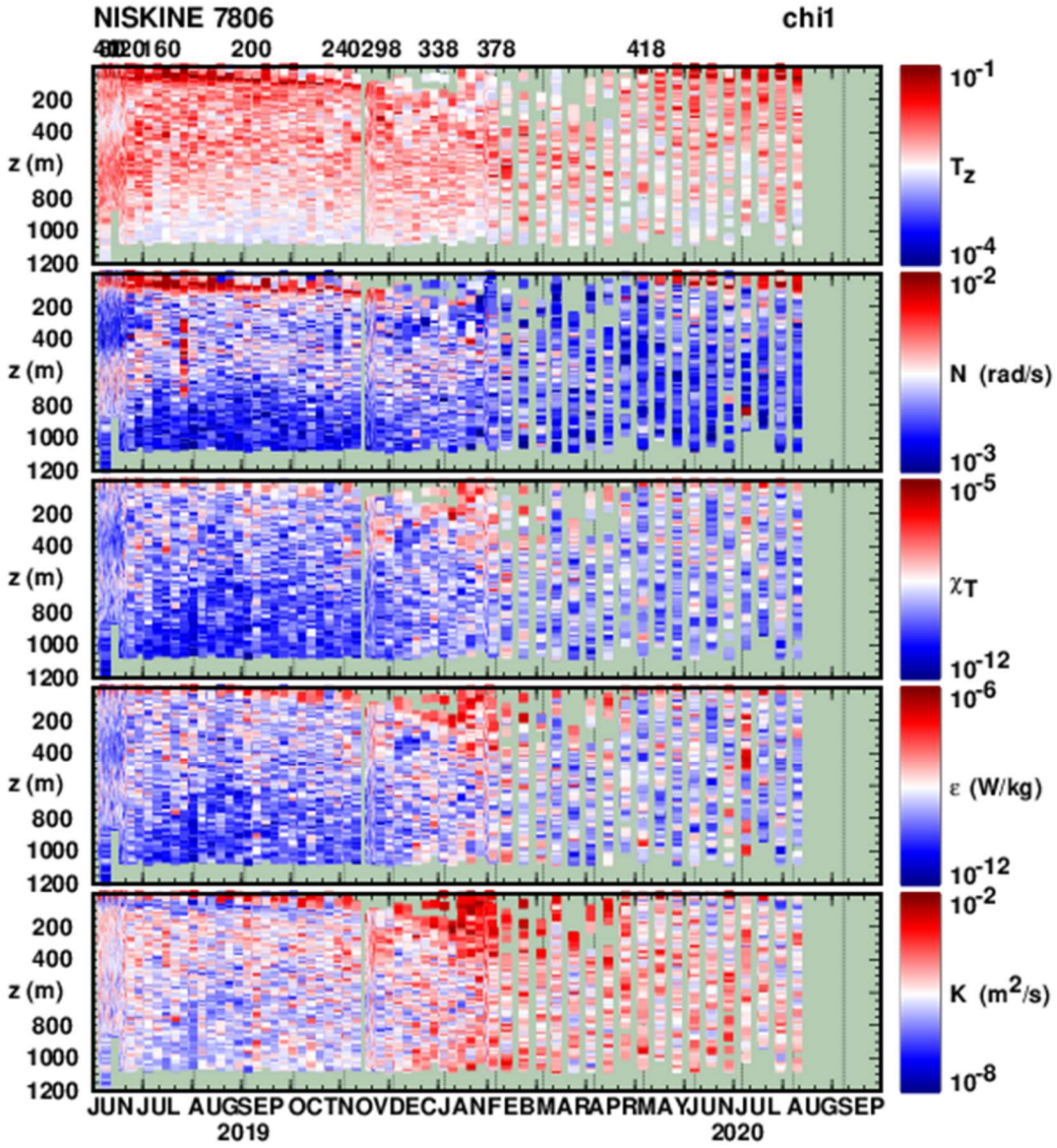
NISKINE 7806
chi1
JUN JUL AUG SEP OCT NOV DEC JAN FEB MAR APR MAY JUN JUL AUG SEP
2019
2020
z (m)
200
400
800
1000
1200
10^{-1}
T_z
10^{-4}
10^{-2}
N (rad/s)
10^{-3}
10^{-5}
χ_T
10^{-12}
10^{-6}
ε (W/kg)
10^{-12}
10^{-2}
K (m^2/s)
10^{-8}

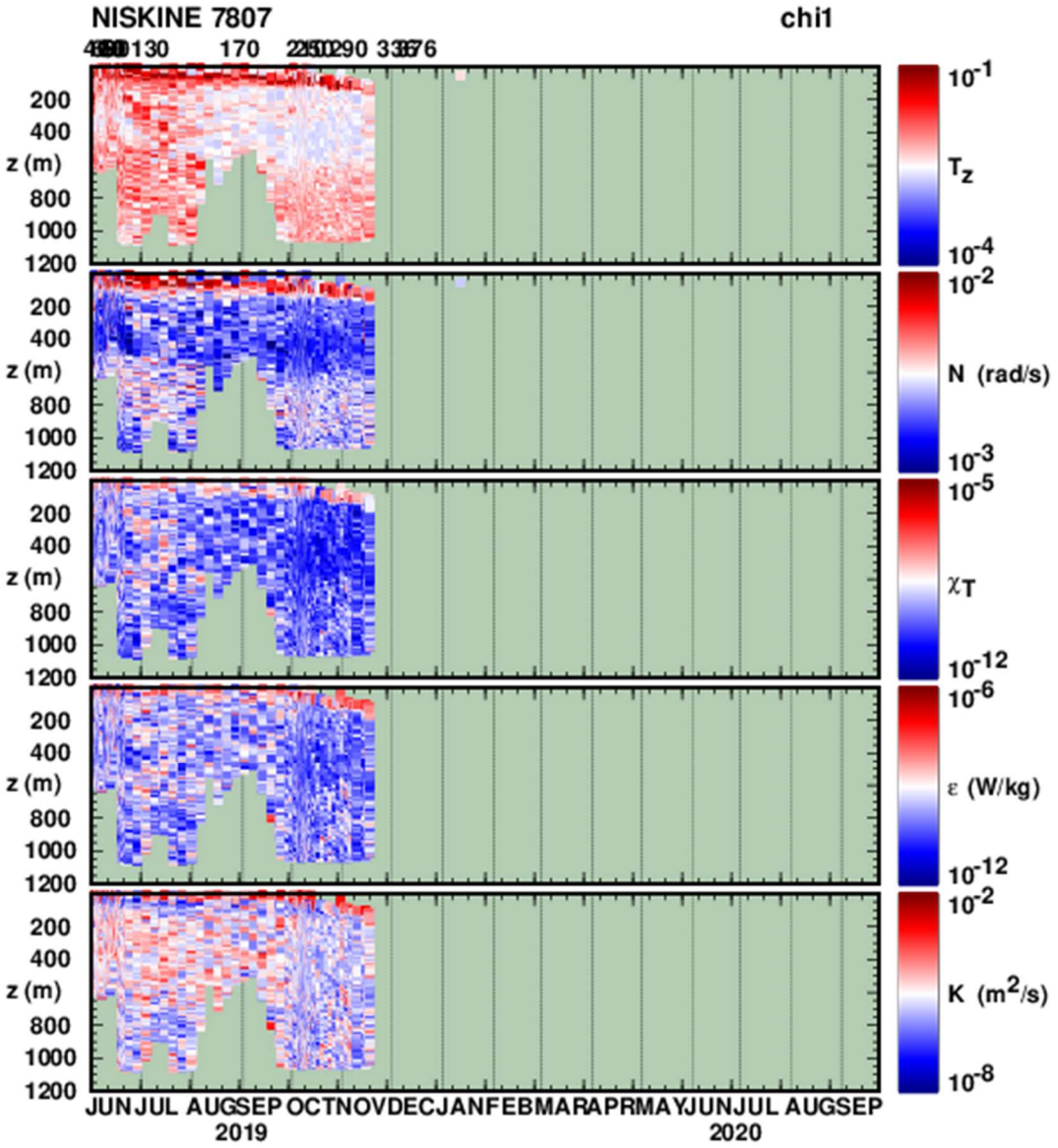
NISKINE 7807
chi1
z (m)
200
400
800
1000
1200
JUN JUL AUG SEP OCT NOV DEC JAN FEB MAR APR MAY JUN JUL AUG SEP
2019
2020
10^{-1}
T_z
10^{-4}
10^{-2}
N (rad/s)
10^{-3}
10^{-5}
χ_T
10^{-12}
10^{-6}
ε (W/kg)
10^{-12}
10^{-2}
K (m^2/s)
10^{-8}

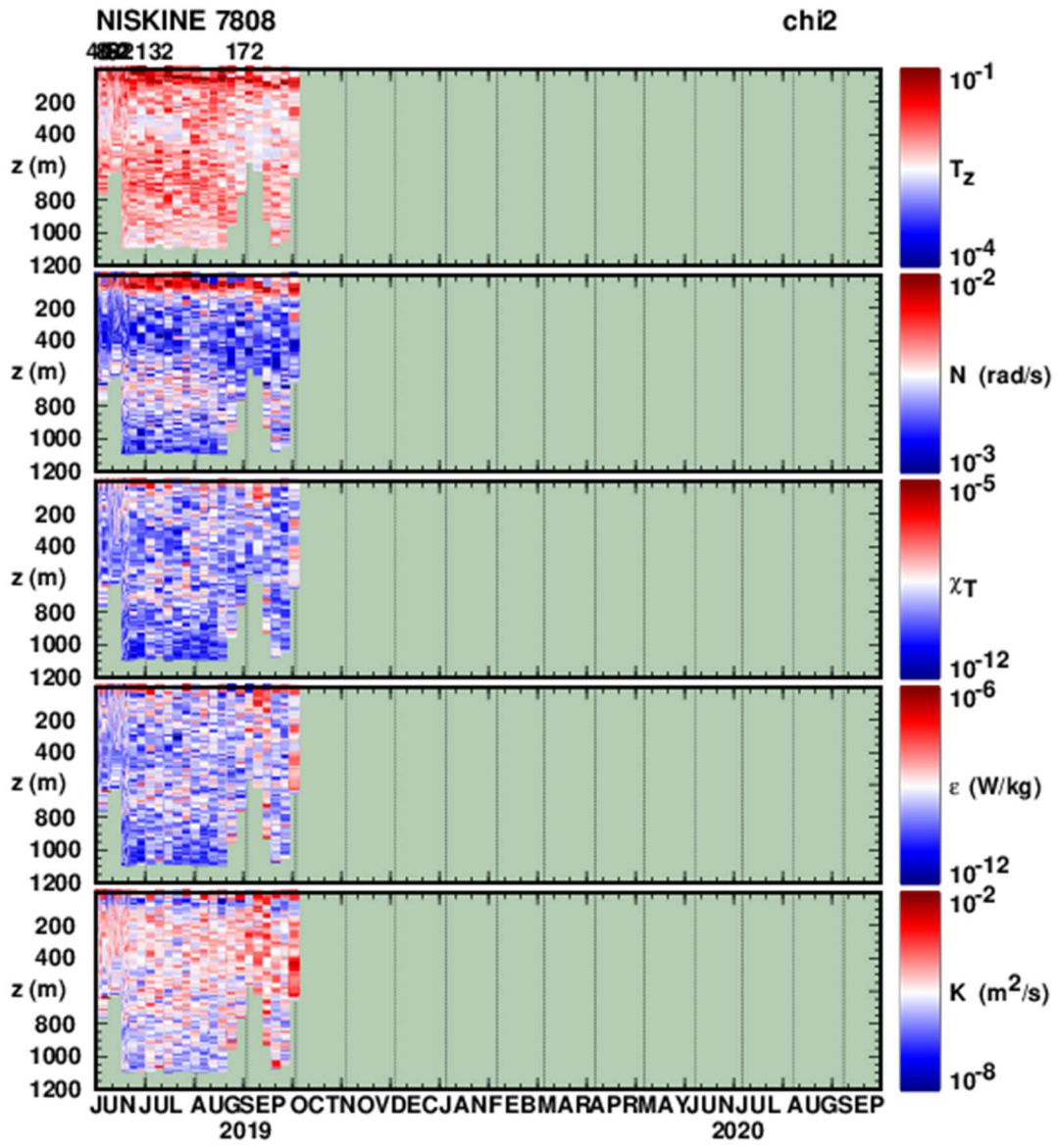

Fig. 6: As in Fig. 5 but for the 6 EM floats that were left behind.

Appendix B: PDFs, Time-Average Depth Profiles and Depth-Average Time-Series by Sensor:

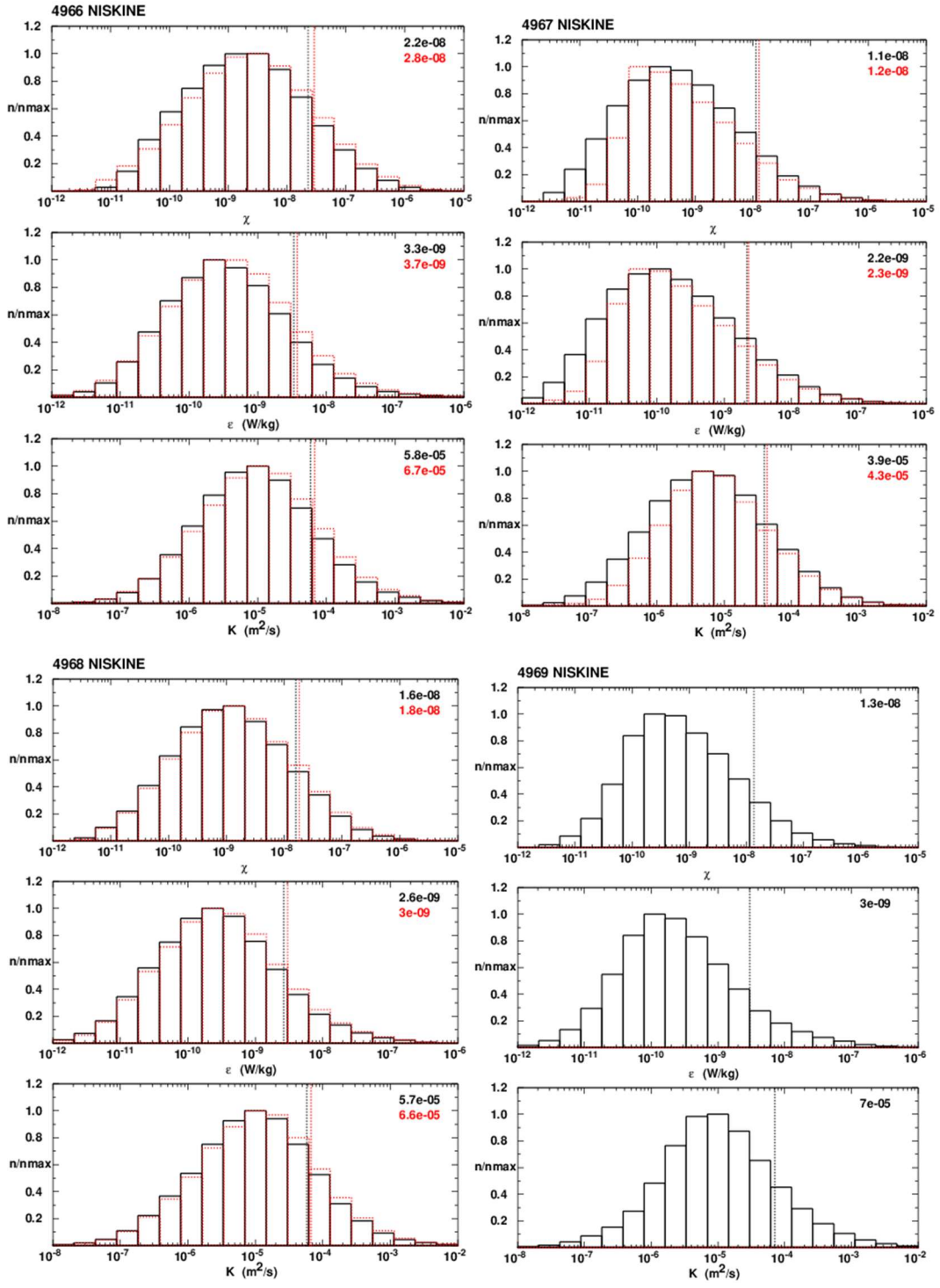

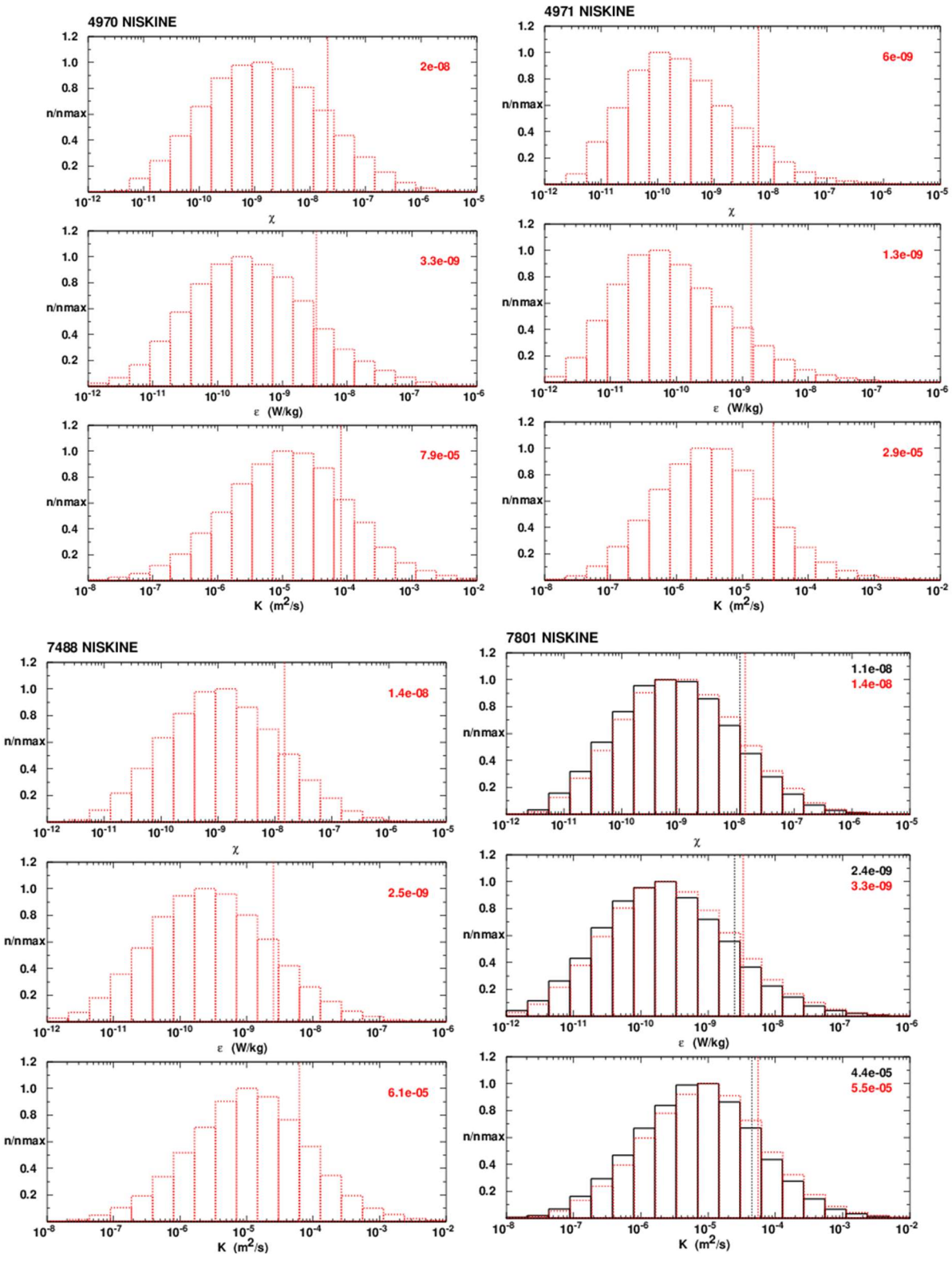
4970 NISKINE
2e-08
3.3e-09
7.9e-05
4971 NISKINE
6e-09
1.3e-09
2.9e-05
7488 NISKINE
1.4e-08
2.5e-09
6.1e-05
7801 NISKINE
1.1e-08
1.4e-08
2.4e-09
3.3e-09
4.4e-05
5.5e-05
n/nmax
χ
ε (W/kg)
K (m2/s)

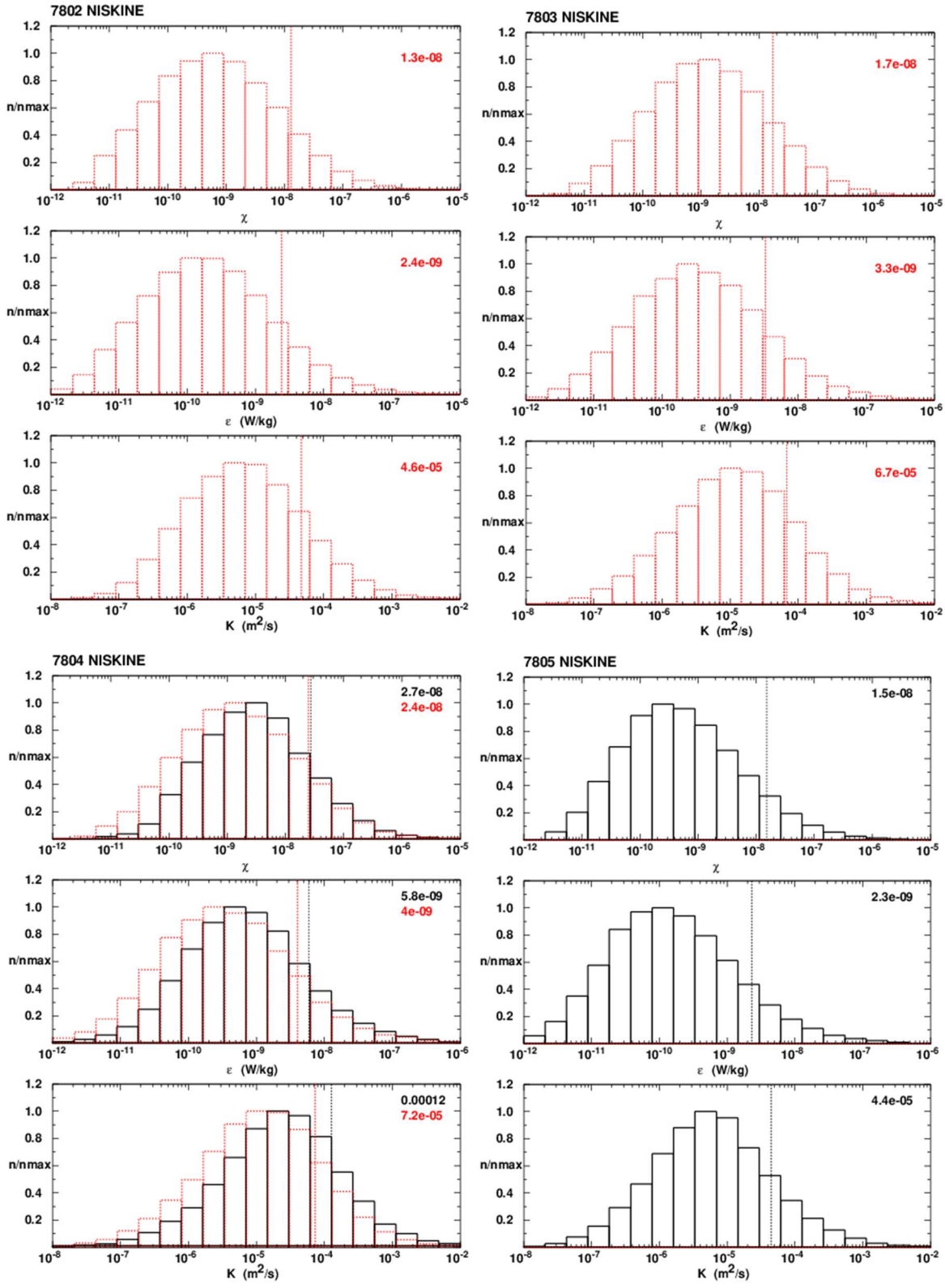
7802 NISKINE
1.3e-08
2.4e-09
4.6e-05
7803 NISKINE
1.7e-08
3.3e-09
6.7e-05
7804 NISKINE
2.7e-08
2.4e-08
5.8e-09
4e-09
0.00012
7.2e-05
7805 NISKINE
1.5e-08
2.3e-09
4.4e-05
n/nmax
χ
ε (W/kg)
K (m2/s)

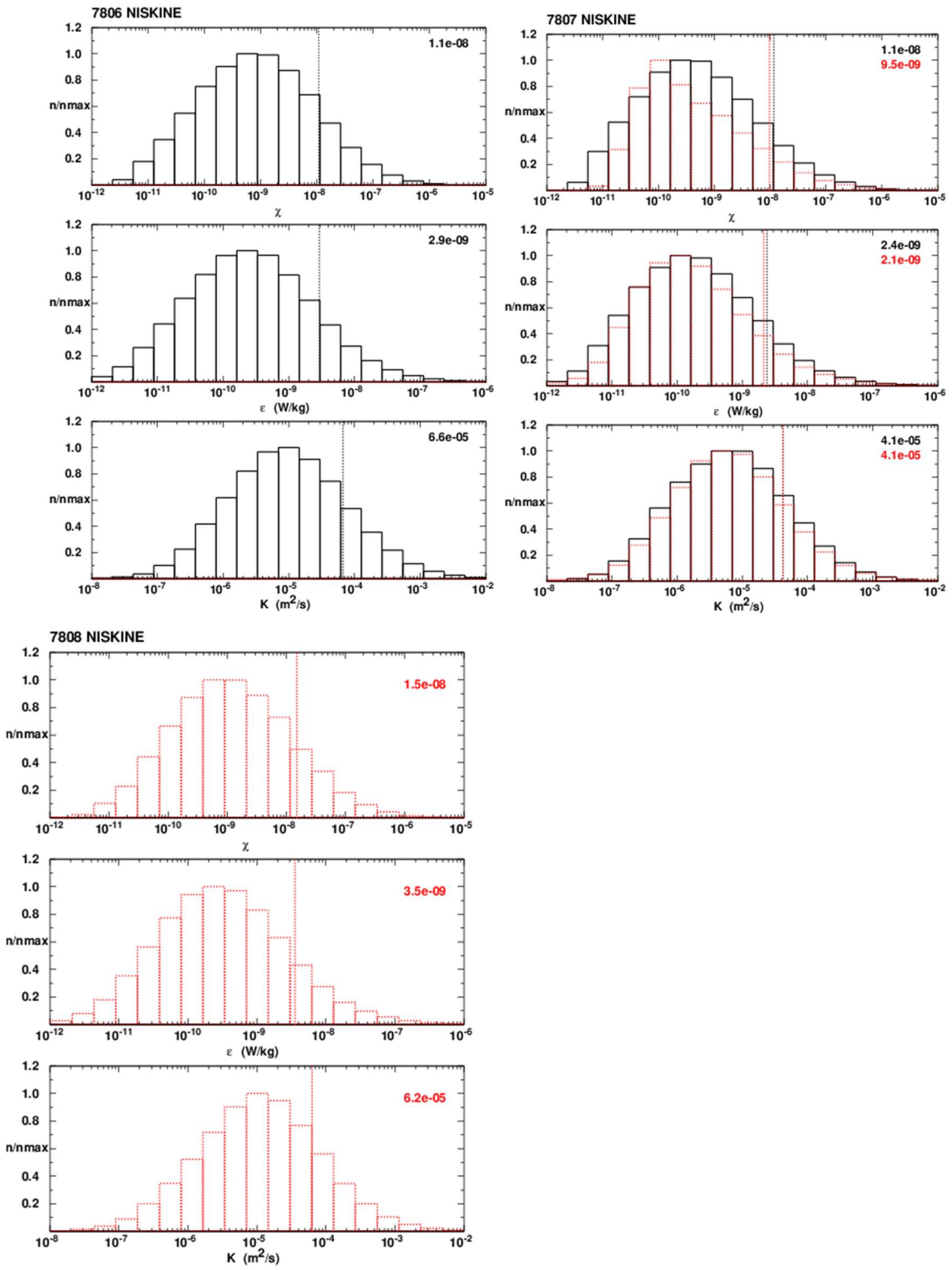

Fig. 7: PDFs of χ_T, ε and K_T from all float chi sensors. Black is from chi1, red chi2. Sensor data was excluded from averages (Figs. 1 and 2) if its PDF was not lognormal even if its mean was similar to or smaller than that of the other sensor, e.g. float 7802.

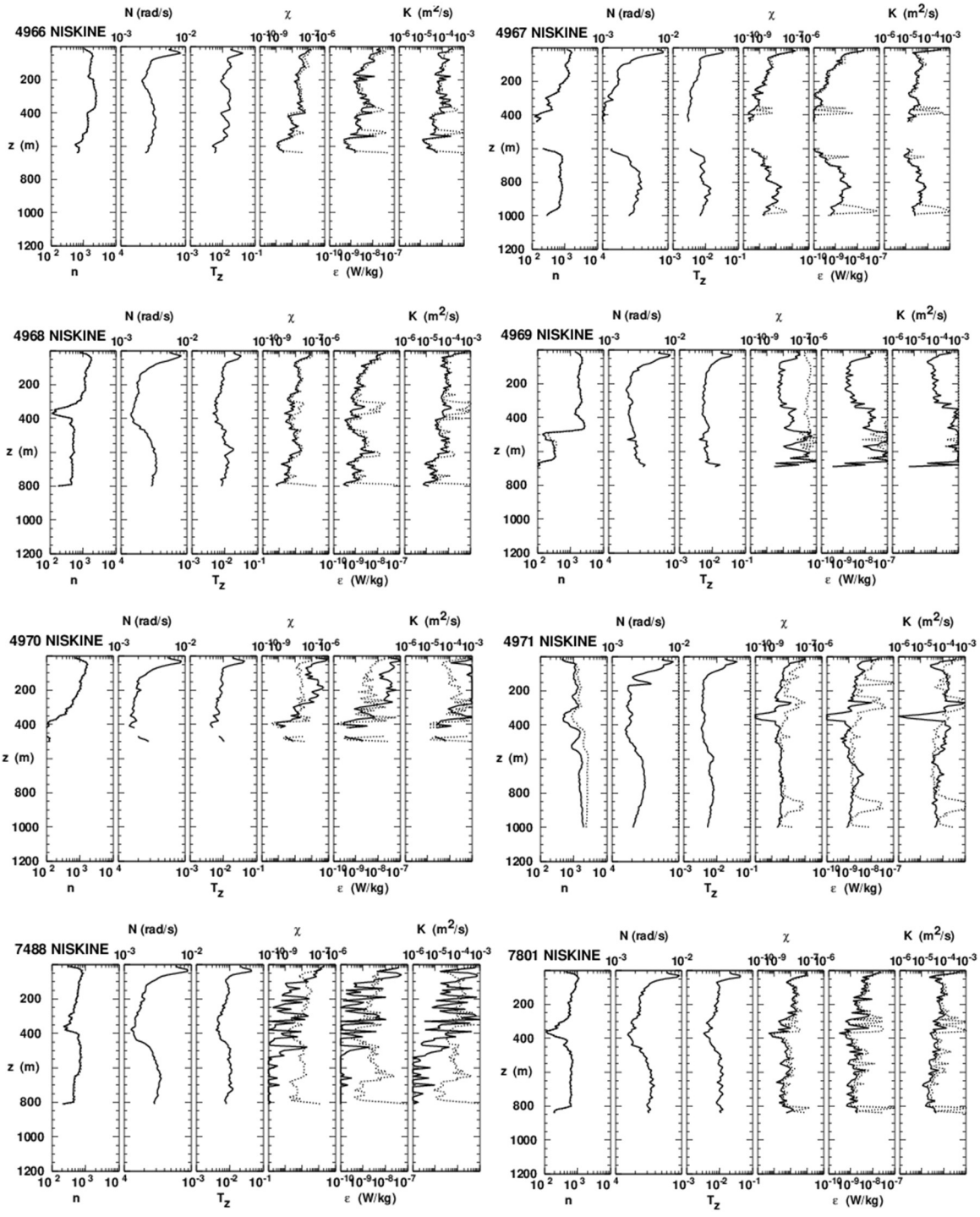
4966 NISKINE
4967 NISKINE
4968 NISKINE
4969 NISKINE
4970 NISKINE
4971 NISKINE
7488 NISKINE
7801 NISKINE
N (rad/s)
χ
K (m²/s)
z (m)
n
T_z
ε (W/kg)

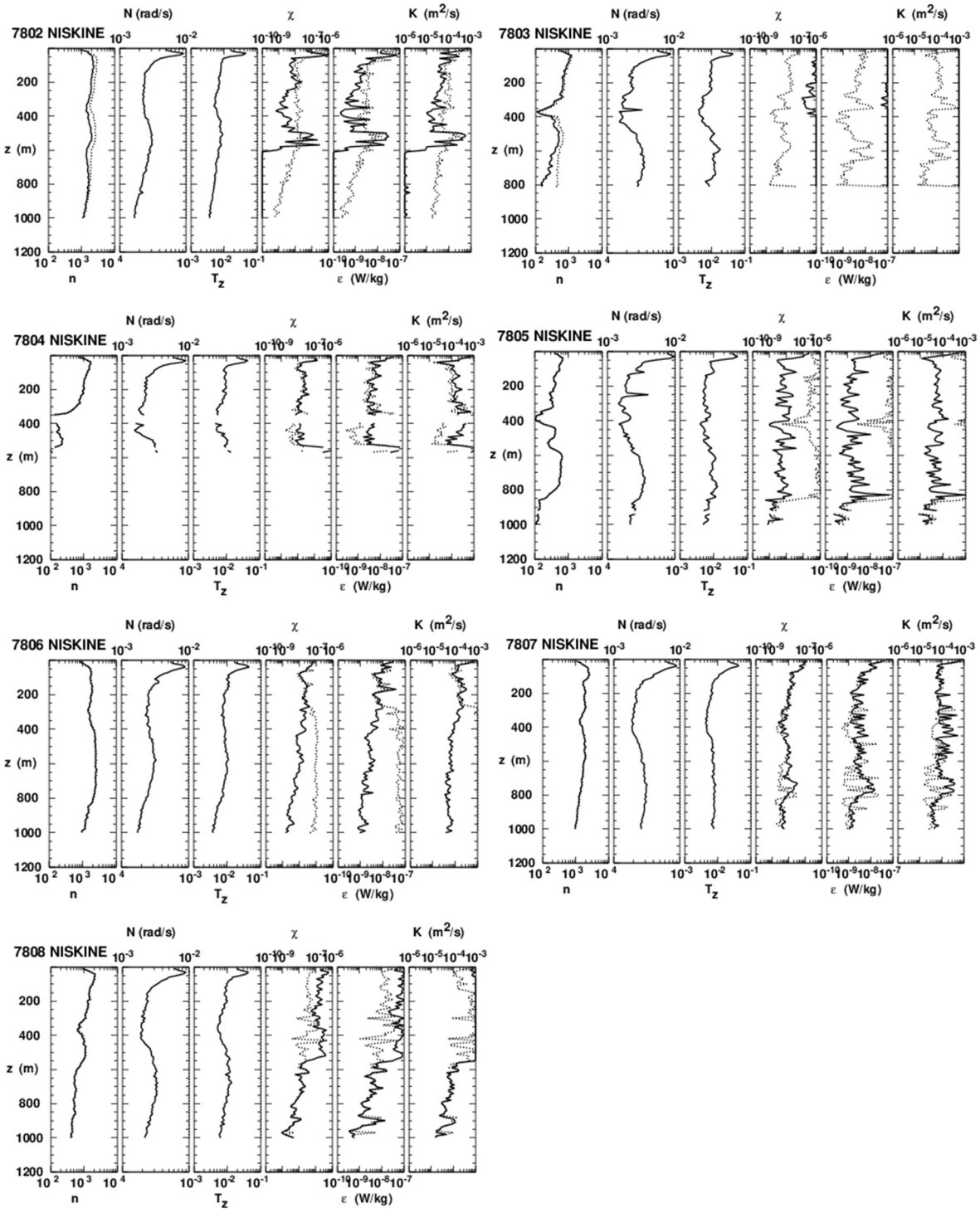

Fig. 8: Average profiles of n, buoyancy frequency N, temperature-gradient T_z, χ_T, ε and K_T for each float chi sensor. Solid is sensor chi1, dotted chi2. Sensor data was excluded from averages (Figs. 1 and 2) if its profile was atypical, e.g. both 4969 sensors, and 7488 and 7802 chi1.

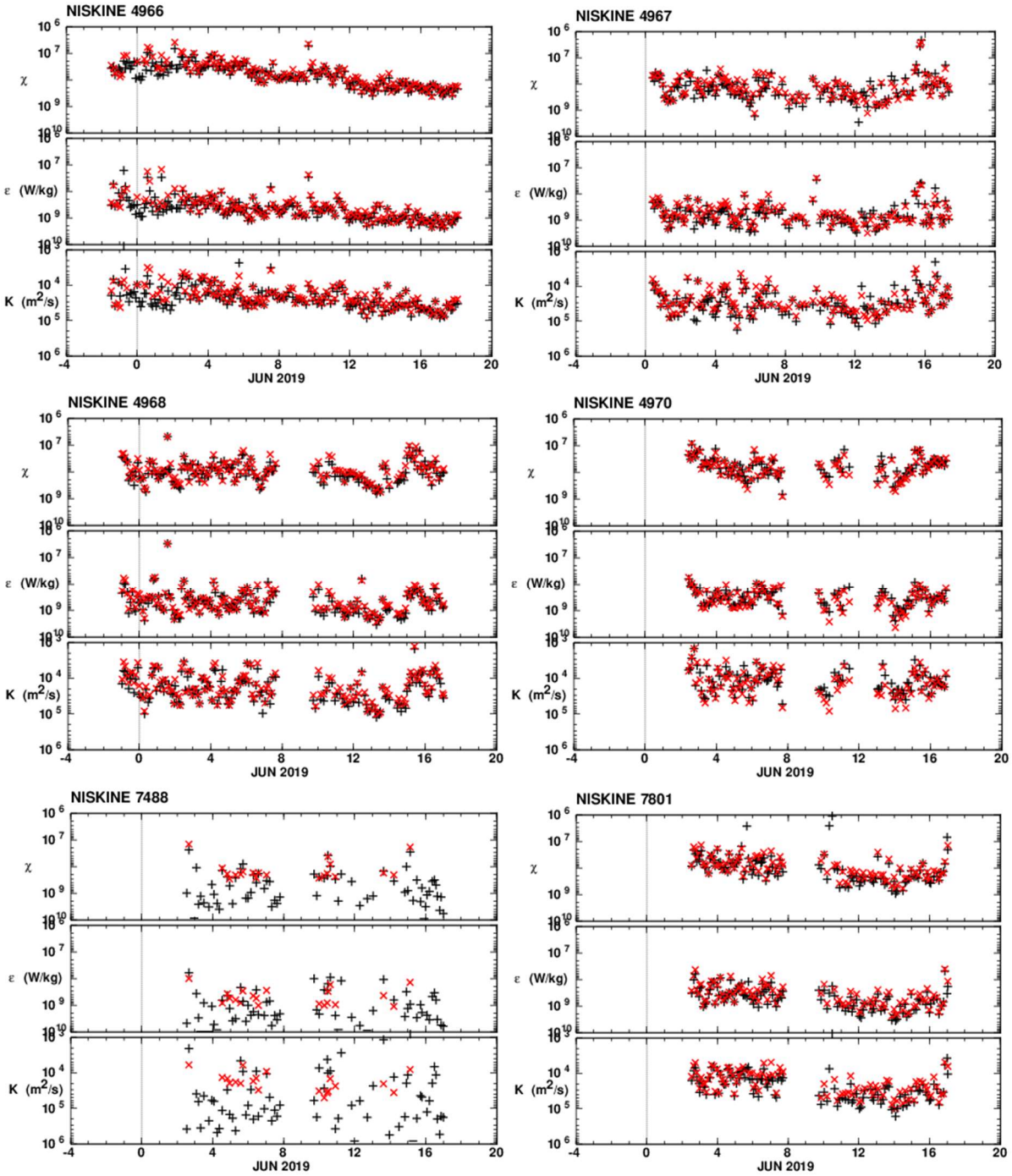
NISKINE 4966
NISKINE 4967
NISKINE 4968
NISKINE 4970
NISKINE 7488
NISKINE 7801
χ
ε (W/kg)
K (m²/s)
JUN 2019

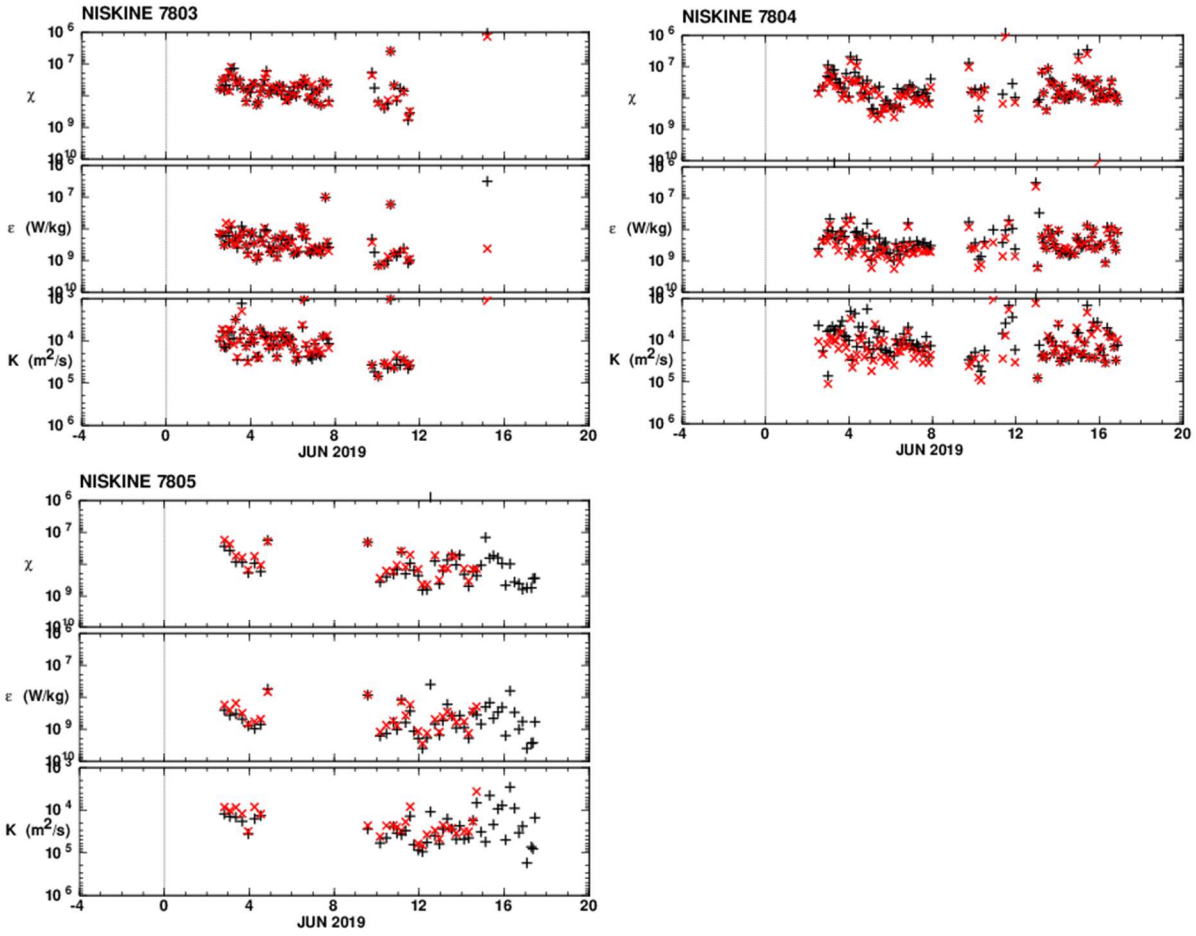

Fig. 9: Time-series of depth-average χ_T, ε and K_T from the floats deployed during the JUN 2019 process cruise. Data were not included in the averages if $N^2 < 4f^2$ or $T_z < 0.002$ °C/m. Microstructure tends to be higher near the beginning of the month because of a storm in late MAY 2019 and lower toward the end.

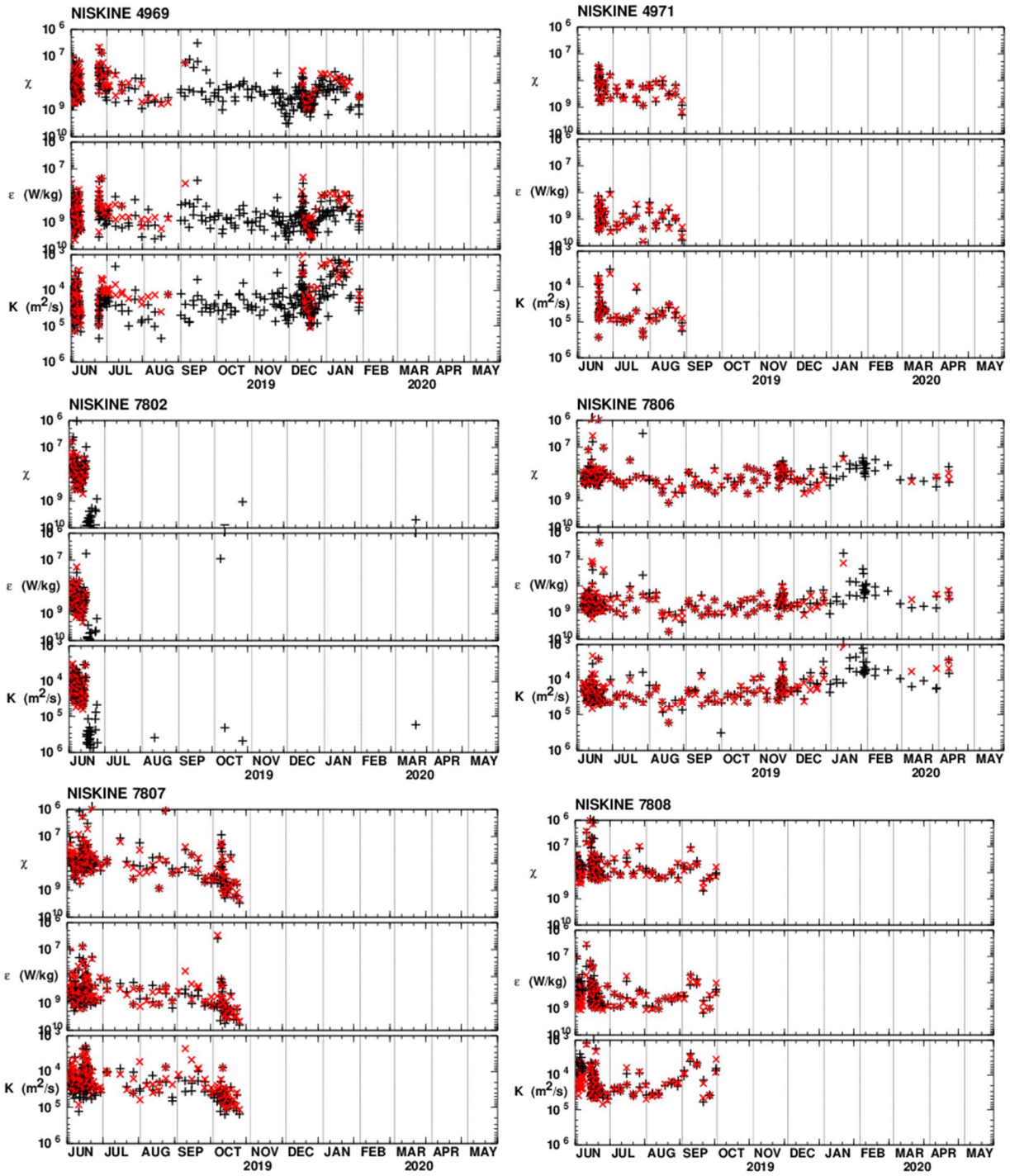

Fig. 10: As in Fig. 9 but for the long deployment. There is a brief maximum in early SEP (storm? shoaling topography?) then a gradual increase by an order of magnitude through fall and early winter til late JAN 2020 followed by a decrease.